Molecular Biology of the Cell
Vol. 11, 2297–2313, July 2000

Insights into the Structural Organization of the I1 Inner Arm Dynein from a Domain Analysis of the 1β Dynein Heavy Chain

Catherine A. Perrone,* Steven H. Myster,*† Raqual Bower,* Eileen T. O'Toole,‡ and Mary E. Porter*§

*Department of Genetics, Cell Biology, and Development, University of Minnesota Medical School, Minneapolis, Minnesota 55455; and ‡Department of Molecular, Cellular, and Developmental Biology, University of Colorado at Boulder, Boulder, Colorado 80309

Submitted February 24, 2000; Revised April 7, 2000; Accepted April 20, 2000
Monitoring Editor: Thomas D. Pollard

To identify domains in the dynein heavy chain (Dhc) required for the assembly of an inner arm dynein, we characterized a new motility mutant (*ida2-6*) obtained by insertional mutagenesis. *ida2-6* axonemes lack the polypeptides associated with the I1 inner arm complex. Recovery of genomic DNA flanking the mutation indicates that the defects are caused by plasmid insertion into the *Dhc10* transcription unit, which encodes the 1β Dhc of the I1 complex. Transformation with *Dhc10* constructs encoding <20% of the Dhc can partially rescue the motility defects by reassembly of an I1 complex containing an N-terminal 1β Dhc fragment and a full-length 1α Dhc. Electron microscopic analysis reveals the location of the missing 1β Dhc motor domain within the axoneme structure. These observations, together with recent studies on the 1α Dhc, identify a Dhc domain required for complex assembly and further demonstrate that the intermediate and light chains are associated with the stem regions of the Dhcs in a distinct structural location. The positioning of these subunits within the I1 structure has significant implications for the pathways that target the assembly of the I1 complex into the axoneme and modify the activity of the I1 dynein during flagellar motility.

INTRODUCTION

The dyneins are a family of molecular motors that convert the chemical energy of ATP binding and hydrolysis into mechanical force, resulting in minus-end–directed movement along microtubules. These motors play important roles in a number of diverse cellular processes, including mitotic events, vesicle movement, and ciliary and flagellar motility (Mitchell, 1994; Porter, 1996; Hirokawa *et al.*, 1998). All dynein isoforms characterized thus far are large, multisubunit complexes containing one to three dynein heavy chains (Dhcs) (400–500 kDa), variable numbers of intermediate chains (ICs) (45–140 kDa), and one or more light chains (LCs) (8–28 kDa). Dyneins can be separated into two different classes: cytoplasmic and axonemal. Axonemal dynein isoforms are much more diverse, e.g., in *Chlamydomonas*, as many as seven different inner dynein arm isoforms have been identified, along with one three-headed outer arm isoform (Goodenough *et al.*, 1987; Kagami and Kamiya, 1992). Despite this diversity, several of the axonemal Dhcs, ICs, and LCs share considerable homology with their cytoplasmic counterparts (Mitchell and Brown, 1994; Wilkerson *et al.*, 1994, 1995; King and Patel-King, 1995; Harrison *et al.*, 1998; Yang and Sale, 1998).

Axonemal dyneins have been studied most extensively in *Chlamydomonas* because of its accessibility to combined genetic, biochemical, and structural analysis (Harris, 1989, Goodenough, 1992; Dutcher, 1995). *Chlamydomonas* is haploid, and so it is relatively easy to screen for mutations in motility genes and thereby evaluate the contribution of each dynein isoform to flagellar motility. The ability to reintroduce modified dynein genes by transformation also allows for the investigation of functional domains within dynein subunits (Perrone *et al.*, 1998; Myster *et al.*, 1999). Furthermore, because each dynein isoform is targeted to a specific location within the 96-nm axoneme repeat, wild-type and mutant axonemes can be compared to determine in situ the structural alterations that result from specific polypeptide

† Present address: Department of Biology, Coker Hall, CB#3280, University of North Carolina at Chapel Hill, Chapel Hill, NC 27599-3280.
§ Corresponding author. E-mail address: mary-p@biosci.cbs.umn.edu.
Abbreviations used: BAC, bacterial artificial chromosome; Dhc, dynein heavy chain; IC, intermediate chain; LC, light chain; P-loop, phosphate-binding motif; RFLP, restriction fragment length polymorphism; RT, reverse transcriptase.

Table 1. Characteristics of motility mutants used in this study

Strain name	Dynein defect	Motility	Swimming velocity (μm/s, n > 40)	Ability to phototax	Reference
Wild type (137c)	None	Wild type	144.2 ± 17.1[a]	Yes	Harris, 1989
pf28	Outer arm	Slow, jerky swimming	51.5 ± 6.9[b]	Yes	Mitchell and Rosenbaum, 1985
pf9-2	I1 complex	Slow, smooth swimming	73.4 ± 12.4[b]	No	Porter et al, 1992
pf9-3	Il complex	Slow, smooth swimming	72.3 ± 14.1[b]	No	Myster et al., 1997
ida3-1	I1 complex	Slow, smooth swimming	77.3 ± 11.0[c]	No	Kamiya et al., 1991
ida7-1	I1 complex	Slow, smooth swimming	81.5 ± 14.0[a]	No	Perrone et al., 1998
ida2-1	I1 complex	Slow, smooth swimming	77.7 ± 15.2[c]	No	Kamiya et al., 1991
ida2-6 (27B3)	I1 complex	Slow, smooth swimming	77.6 ± 15.4[a]	No	Perrone et al., 1998; this study
ida2-6::λC (D11)	1β Dhc	Faster swimming	107.9 ± 15.3	Yes	This study
ida2-6::λH (9A)	1β Dhc	Faster swimming	ND[d]	Yes	This study
ida2-7 (J6H9)	I1 complex	Slow, smooth swimming	53.7 ± 10.7	No	This study
ida2-7::pCAP1 (B3)	1β Dhc	Faster swimming	91.8 ± 12.6	Yes	This study
ida2-7::pCAP3 (B6)	1β Dhc	Faster swimming	74.1 ± 9.9	Yes	This study

[a] Velocity determined by Perrone et al. (1998).
[b] Velocity determined by Myster et al. (1999).
[c] Velocity determined by Kamiya et al. (1991).
[d] ND, not determined.

defects (Piperno *et al.*, 1990; Mastronarde *et al.*, 1992; Gardner *et al.*, 1994). Such studies have provided the experimental evidence that the conserved central and C-terminal portions of the Dhc form the globular head or motor domain, whereas the more divergent N-terminal region forms a stem domain that interacts with associated LCs and ICs (Sakakibara *et al.*, 1993; Myster *et al.*, 1999).

The I1 inner arm complex serves as an excellent model for dynein assembly and function. First, the I1 dynein is a relatively simple isoform that contains two distinct Dhcs, three ICs, and three LCs, and it shares many similarities with the major cytoplasmic dynein. Both are two-headed isoforms that share closely related, WD-repeat containing ICs (Yang and Sale, 1998) and two identical LC subunits (Harrison *et al.*, 1998). One of these LCs (Tctex1) is related to a gene product of the *t* complex, a region of mouse chromosome 17 involved in transmission ratio distortion and male sterility (Lader *et al.*, 1989; Harrison *et al.*, 1998). These observations are consistent with studies in *Chlamydomonas* indicating that the I1 complex is an important target of the regulatory signals that control flagellar movement (Porter *et al.*, 1992; Habermacher and Sale, 1996, 1997; King and Dutcher, 1997). Finally, mutations in four loci that affect the assembly of the I1 complex have been isolated (Kamiya *et al.*, 1991; Porter *et al.*, 1992; Perrone *et al.*, 1998), and in two cases, the mutant gene products have been identified. The *PF9/IDA1* locus corresponds to the *Dhc1* gene, which encodes the 1α Dhc (Myster *et al.*, 1997), whereas the *IDA7* locus corresponds to the structural gene for the WD-repeat containing IC140 (Perrone *et al.*, 1998). By introducing constructs of both genes into the appropriate mutant backgrounds, we have been able to identify regions within these polypeptides required for the reassembly of I1 subunits and the restoration of I1 motor activity (Perrone *et al.*, 1998; Myster *et al.*, 1999).

In this study, we have characterized the gene encoding the second Dhc of the complex, the 1β Dhc, to assess its role in the assembly and targeting of the I1 complex. Using an I1 mutant strain obtained by insertional mutagenesis, we have shown by complementation analysis that the mutation is an allele (*ida2-6*) at the *IDA2* locus. The recovery of genomic DNA flanking the site of plasmid insertion has further demonstrated that the *ida2-6* mutation is a defect in the *Dhc10* gene. Transformation of *ida2* with truncated constructs of the *Dhc10* gene can partially rescue the mutant defects. The 1β Dhc fragment encoded by the truncated transgene represents <20% of the full-length Dhc, yet it still supports the assembly of other I1 complex subunits onto the axoneme. High-resolution structural analysis of wild-type and mutant axonemes has revealed the location of the missing 1β Dhc motor domain within the structure of the I1 complex. This work, together with our previous study of the *Dhc1* gene (Myster *et al.*, 1999), has allowed us to identify the location of the polypeptides that form the major structural domains of the I1 complex in situ and to further define the regions of the Dhc that are required for complex assembly and activity. Given the similarity of the 1β Dhc to other Dhc isoforms, our findings also have implications for the assembly of other dynein complexes.

MATERIALS AND METHODS

Cell Culture, Mutant Strains, and Genetic Analyses

The strains used in this study are listed in Table 1. All strains were maintained as vegetatively growing cultures (Myster *et al.*, 1997, 1999; Perrone *et al.*, 1998). The 27B3 strain (*ida2-6*) was isolated by David Mitchell (State University of New York Medical Center, Syracuse, NY) after transformation of a nit− strain (*nit1-305*) with the pMN24 plasmid containing the wild-type nitrate reductase gene (*NIT1*). 27B3 was identified as a potential I1 mutant as described by Perrone *et al.* (1998). J6H9 (*ida2-7*) was isolated by Gerald Rupp in our laboratory after transformation of a nit− strain (A54-e18) with a smaller *NIT1* plasmid, pMN56.

To determine whether the motility defects in 27B3 were linked to the *NIT1* plasmid used as the selectable marker, 27B3 was backcrossed to a nit− strain, and random progeny were analyzed for their ability to grow on selective medium and for their motility

phenotypes. All 46 nit+ progeny had the same slow motility phenotype as the 27B3 strain, whereas all 52 nit− progeny had wild-type motility. These data suggested that the defect in 27B3 was the result of plasmid insertion into a motility gene.

To determine if the 27B3 mutation might be an allele at a previously identified I1 locus (i.e., *PF9/IDA1*, *IDA2*, *IDA3*, or *IDA7*), complementation tests were performed by constructing stable diploid cell lines with the auxotrophic markers *arg2* and *arg7*, as described previously (Ebersold, 1967; Perrone *et al.*, 1998).

Analysis of Motility

Motility phenotypes and swimming velocities were assessed using phase-contrast microscopy and video recordings of live cells (Porter *et al.*, 1992; Perrone *et al.*, 1998). The ability of wild-type and mutant strains to undergo phototaxis was determined using both a tube-based assay (King and Dutcher, 1997) and a microtiter dish–based assay (Myster *et al.*, 1999). A strain was designated phototaxis positive if the majority of swimming cells were concentrated on the lighted side of the tube or microtiter well.

Southern Blot and Northern Blot Analyses

DNA and RNA isolation, restriction enzyme digests, agarose gels, Southern blots, and Northern blots were performed as described previously (Porter *et al.*, 1996, 1999; Myster *et al.*, 1997; Perrone *et al.*, 1998) with minor modifications to our Northern blot protocol to improve sensitivity. Gels were blotted onto a Brightstar (Ambion, Austin, TX) membrane, and Northern blots were prehybridized and hybridized in an Ultrahybe solution (Ambion) containing 100 μg/ml salmon sperm DNA.

Restriction Fragment Length Polymorphism Mapping

To place *Dhc10* on the genetic map, the ~150-base pair (bp) PCR product (Porter *et al.*, 1999) was first used as a probe on genomic Southern blots to identify a restriction fragment length polymorphism (RFLP) between two polymorphic *Chlamydomonas reinhardtii* strains, *137c* and *S1-D2*. An RFLP was easily observed using an *Eco*RI–*Xho*I digest. The *Dhc10* probe was then hybridized to a series of mapping filters containing genomic DNA isolated from tetrad progeny of crosses between multiply marked *C. reinhardtii* strains and *S1-D2*. The segregation of the *Dhc10* RFLP in the tetrad progeny was analyzed with respect to the segregation of more than 42 genetic and molecular markers (Porter *et al.*, 1996).

Electron Microscopy and Image Analysis

Axonemes for electron microscopy were prepared as described previously (Porter *et al.*, 1992). Longitudinal images were digitized, averaged, and compared with the use of the methods described by Mastronarde *et al.* (1992) and O'Toole *et al.* (1995). The final average for each sample contained at least 70 of the 96-nm axoneme repeats.

Protein Purification, SDS-PAGE, and Western Blot Procedures

Large-scale (20–40 l) culture of vegetative cells, the isolation of purified axonemes, and sucrose density gradient centrifugation of dynein extracts were performed as described previously (Porter *et al.*, 1992; Myster *et al.*, 1997, 1999; Perrone *et al.*, 1998). The Dhcs in whole axonemes were resolved on 3–5% polyacrylamide, 3–8 M urea gradient gels (Kamiya *et al.*, 1991). Sucrose density gradient fractions were analyzed on 5–15% polyacrylamide, 0–0.25 M glycerol gradient gels. Dynein LCs were analyzed on 7.0% polyacrylamide gels. Gels were stained with silver (Wray *et al.*, 1981) or transferred to polyvinylidene difluoride or nitrocellulose membranes.

Western blots were incubated as described previously (Myster *et al.*, 1997, 1999; Perrone *et al.*, 1998) with the following antibodies: a rabbit polyclonal antibody generated against an IC140 fusion protein (Yang and Sale, 1998), a rabbit polyclonal antibody raised against a specific peptide in the 1α Dhc sequence (Myster *et al.*, 1997), or a rabbit polyclonal antibody (R5205) generated against a Tctex1 fusion protein derived from a human cDNA library (King *et al.*, 1996). Blots were developed with the use of an alkaline phosphatase–conjugated secondary antibody and either colorimetric (Sigma Chemical, St. Louis, MO) or chemiluminescent detection (Tropix, Bedford, MA).

Recovery of Genomic DNA Flanking the Site of Plasmid Insertion in ida2-6

To recover genomic DNA flanking the site of plasmid insertion, genomic DNA from wild type and *ida2-6* was digested with *Kpn*I, which does not cut within the pMN24 plasmid, and *Cla*I, which digests the pMN24 plasmid at a single site near the 5′ end of the *NIT1* gene. After size fractionation on a 0.8% agarose gel and Southern blotting, the samples were hybridized with an ~11.5-kilobase (kb) fragment of the *NIT1* gene to identify those fragments derived from the endogenous *NIT1* gene present in both samples as well as additional bands corresponding to the inserted *NIT1* plasmids in *ida2-6*. Analysis of the restriction patterns identified a unique 3.4-kb *Kpn*I–*Cla*I fragment in *ida2-6* that was likely to contain genomic DNA flanking the site of plasmid insertion. (Any unique band in *ida2-6* that decreased in size in the double digest must represent a *Kpn*I site present in flanking genomic DNA.) The 3.4-kb *Kpn*I–*Cla*I fragment was cloned by screening a size-fractionated mini library with the *NIT1* sequence, and one plasmid, p27B3, was selected for further analysis.

To identify the region containing only flanking genomic DNA, p27B3 was digested with several enzymes and rehybridized with the *NIT1* gene. A 350-bp *Kpn*I–*Sau*3A fragment that failed to hybridize with the *NIT1* sequence was identified as potential flanking genomic DNA. To verify that this fragment was derived from the region flanking the site of plasmid insertion, the 350-bp fragment was rehybridized to a Southern blot of wild-type and *ida2-6* genomic DNA.

Characterization of Genomic Clones in the IDA2/Dhc10 Region

To recover a wild-type copy of the *IDA2* gene, the 350-bp *Kpn*I–*Sau*3A fragment of p27B3 was used to screen a large-insert, wild-type genomic strain (21gr) library constructed in λFIXII (Schnell and Lefebvre, 1993), as described previously (Porter *et al.*, 1996, 1999; Myster *et al.*, 1997), and seven overlapping phage clones were identified. Four additional clones were obtained by screening the library with the 150-bp product of the Dhc10 gene. Additional flanking genomic DNA was obtained using a reverse transcriptase (RT)-PCR product derived from one end of the phage walk to screen a *Chlamydomonas* bacterial artificial chromosome (BAC) library (Genome Systems, St. Louis, MO) and recover five overlapping BAC clones, as described previously (Myster *et al.*, 1999).

To test the ability of the phage clones to rescue the motility defect in *ida2-6*, an *ida2-6 arg2* strain was cotransformed with 1–3 μl of phage DNA and 2 μg of the *Bam*HI-linearized plasmid pARG7.8 (Debuchy *et al.*, 1989) by means of the glass bead–mediated transformation protocol (Kindle, 1990; Nelson and Lefebvre, 1995; Perrone *et al.*,1998). Arg+ transformants were selected by plating on Tris-acetate-phosphate medium lacking arginine. After growth for 7–10 d, transformant lines were picked into liquid Tris-acetate-phosphate medium and screened for rescue of the *ida2-6* motility defect on a dissecting microscope. A total of 150–300 transformants were screened per clone. Rescued strains were restreaked for single colonies and rescored by phase-contrast microscopy.

To identify the minimum region required to rescue the *ida2* mutant phenotype, a 17.1-kb *Xba*I fragment from phage clone C was ligated into pBluescript KS II to obtain the subclone pCAP1. pCAP2 was obtained by isolating an ~4.6-kb *Bgl*I fragment from pCAP1 and ligating into a *Hin*cII-digested plasmid. pCAP3 was obtained by isolating an ~14-kb *Bgl*II fragment from pCAP1 and ligating into a *Bam*HI-digested plasmid. pCAP1 encodes up to amino acid residue 989 of the *Dhc10* sequence, followed by the addition of 8 novel amino acids (ESTPFSEG); pCAP2 encodes up to residue 508, followed by 4 amino acids (GRYR); and pCAP3 encodes up to residue 811, followed by 2 amino acids (IH).

Sequencing the Dhc10 Gene

Selected subclones were sequenced by primer walking at the DNA sequencing facility at Iowa State University (Ames, IA). The sequence data were assembled and analyzed using the Genetics Computer Group (GCG; Madison, WI) software, version 9.0, and the MacVector Sequence Analysis Software, version 6.0 (International Biotechnologies, Rochester, NY). Potential ORFs and splice sites were identified with the use of codon usage tables (Nakamura *et al.*, 1997) and the consensus donor and acceptor sequences found in *Chlamydomonas* nuclear genes (Mitchell and Brown, 1994; LeDizet and Piperno, 1995; Zhang, 1996). All splice junctions were confirmed by sequencing RT-PCR products amplified with gene-specific primers designed to span intron–exon boundaries, as described previously (Myster *et al.*, 1999; Porter *et al.*, 1999). We were unable to sequence a small region of genomic DNA (~700 bp) in the middle of the 4.7-kb *Sac*I subclone, but we were able to sequence a 354-bp RT-PCR product spanning the gap. The sequence of the *Dhc10* transcription unit (~25 kb) is available under three linked accession numbers (AJ242523–AJ242525).

The predicted amino acid sequence of the *Dhc10* gene product was analyzed using the GCG programs Bestfit, Compare, Pileup, Dotplot, and Motifs, as described previously (Myster *et al.*, 1999; Porter *et al.*, 1999). The COILS program, version 2.2 (Lupus *et al.*, 1991; Lupus, 1996), was used to analyze regions of the amino acid sequence for their potential to form α-helical coiled coils.

Generation of a Specific Antibody for the Dhc10 Gene Product

Sequence alignment of *Chlamydomonas* axonemal Dhcs indicated that the *Dhc10* gene product shared a high degree of sequence similarity with other Dhcs. However, small regions of sequence divergence could be identified in the N-terminal third of the Dhc. Two regions were chosen as sites for peptide synthesis and antibody production, residues 1–15 (MEPGDEGKGHQLTAD) and residues 945–959 (VALQLTDKQRRDMED). The peptides were coupled to keyhole limpet hemocyanin and injected separately into rabbits by Research Genetics (Huntsville, AL). A strong response against the second peptide was detected by ELISA. The antisera were pooled, affinity-purified on a peptide column, and then affinity-purified on Western blots of inner arm dynein extracts, as described previously (Myster *et al.*, 1997, 1999; Perrone *et al.*, 1998).

RESULTS

Identification of a New Axonemal Dhc Gene Linked to the IDA2 Locus

Recent studies have identified four new *Dhc* sequences in *Chlamydomonas*, and comparison with previously identified *Dhc* genes suggested that two of the genes (*cDhc1a* and *cDhc1b*) encode cytoplasmic Dhcs, whereas the other two sequences (*Dhc10* and *Dhc11*) share homology with axonemal Dhc sequences (Porter *et al.*, 1999). In particular, *Dhc10* appears to be most closely related to *Dhc1*, which encodes the 1α Dhc of the inner dynein arm I1 complex (Figure 1A). This homology suggested that *Dhc10* might encode the second Dhc of the I1 complex, known as the 1β Dhc. Mutations in *Dhc10*, therefore, might be expected to disrupt the assembly of the I1 complex and produce an I1 mutant phenotype.

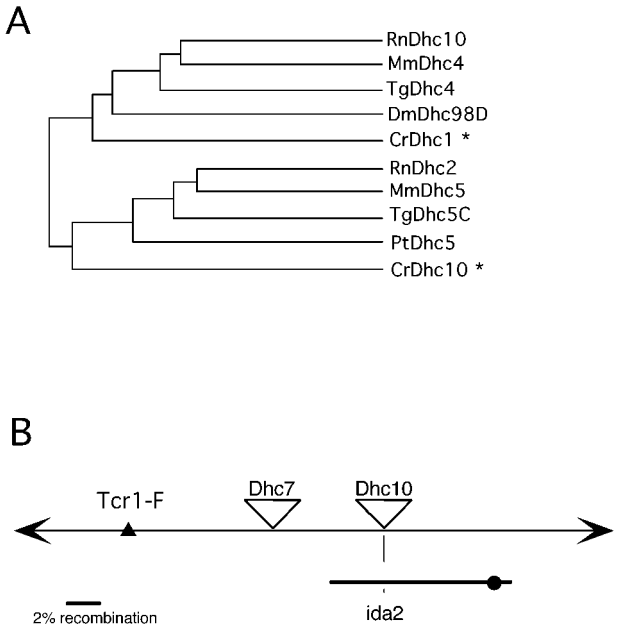

Figure 1. Dendrogram of Dhc sequences and mapping of the *Dhc10* gene. (A) The deduced amino acid sequences surrounding the conserved ATP hydrolytic site (P-loop 1) were aligned with the GCG program Pileup. The subset of Dhc sequences most closely related to *Dhc1* is shown here. The *Chlamydomonas reinhardtii* (Cr) Dhc1 (U61364, AF243806) and Dhc10 (AJ132799) sequences are marked by asterisks. The GenBank accession numbers for the other sequences are as follows: *Tripneustes gratilla* (Tg), U03976, U03973; *Rattus norvegicus* (Rn), D26502, D26493; *Mus musculus* (Mm), Z83812, Z83813; *Paramecium tetraurelia* (Pt) L18803; *Drosophila melanogaster* (Dm) L23200. (B) Genetic map location of the *Dhc10* gene. The *Dhc10* gene was mapped to linkage group XV based on linkage to the genetic marker *ida2* (<2.6 cM, no recombinants in 18 tetrads) and the molecular marker *Dhc7* (~7.4 cM).

To determine whether the *Dhc10* gene is linked to any previously identified I1 mutations, we used RFLP mapping procedures to place *Dhc10* on the genetic map of *Chlamydomonas*. The RFLP data indicated that *Dhc10* maps to linkage group XV, ~7.4 cM from another Dhc locus, *Dhc7*, and less than 2.6 cM from the *ida2* mutation (Figure 1B). Given recent estimates on the physical relationship between the molecular and genetic maps (Silflow, 1998), these results placed *Dhc10* within ~260 kb of the *IDA2* locus.

Isolation of a Tagged ida2 Allele by Insertional Mutagenesis

Although the RFLP data indicated that *Dhc10* and *IDA2* are closely linked, they were not sufficient to identify them as the same locus. However, it is possible to isolate tagged motility mutations in *Chlamydomonas* with the use of inser-

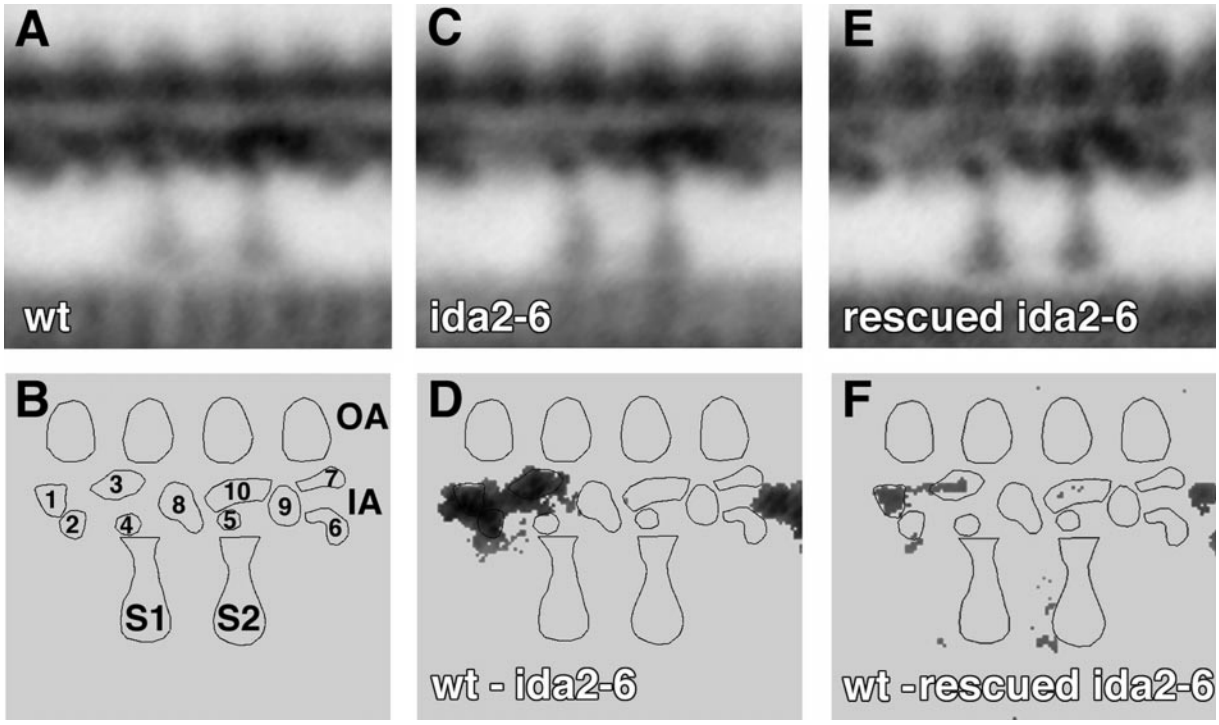

Figure 2. Inner arm structure in wild-type and mutant strains. Longitudinal images of the 96-nm axoneme repeat from wild type, *ida2-6*, and the rescued *ida2-6* strain, D11, are shown here. The averages for wild type (A), *ida2-6* (C), and the rescued *ida2-6* strain (E) are based on 8, 10, and 9 individual axonemes and 74, 87, and 85 axoneme repeats, respectively. (B) Model of the 96-nm axoneme repeat with the major lobes of density in the inner arm region labeled 1–10. The outer arms (OA) are on top, the inner arm (IA) region is below, and the proximal and distal radial spokes are labeled S1 and S2, respectively. (D) Difference plot between wild type and *ida2-6*. (F) Difference plot between wild type and the rescued *ida2-6* strain. The difference plots are derived from a pixel-by-pixel analysis of variance between averages, where statistically significant differences between the averages for two strains are indicated by the gray areas. Differences not significant at the 0.005 confidence level have been set to zero.

tional mutagenesis procedures (Tam and Lefebvre, 1993) and to screen genomic DNA for defects in specific genes. We have used this approach to identify mutations in the *Dhc1*, *IC140*, and *cDhc1b* genes (Myster *et al.*, 1997; Perrone *et al.*, 1998; Porter *et al.*, 1999). During the course of these studies, we recovered a new strain, 27B3, with an I1-like motility phenotype by virtue of its slow swimming speed and its failure to phototax (Perrone *et al.*, 1998). Cosegregation tests have since confirmed that the 27B3 motility phenotype is linked to the inserted *NIT1* plasmid used as a selectable marker (see MATERIALS AND METHODS). Complementation tests have further demonstrated that 27B3 represents a new mutant allele at the *IDA2* locus, now referred to as *ida2-6*. Diploid strains containing 27B3 and the *pf9-2*, *ida3-1*, or *ida7-1* mutation had wild-type motility, whereas diploid strains containing both 27B3 and the *ida2-1* mutation had the slow-motility phenotype characteristic of the parent strains. Therefore, we characterized the phenotype of the *ida2-6* mutant to determine if the assembly of the I1 complex is disrupted and whether the mutant phenotype is a result of a defect in the *Dhc10* gene.

ida2-6 Axonemes Lack the I1 Dynein Complex

To determine if the I1 complex is defective in *ida2-6* axonemes, we isolated axonemes from both *ida2-6* and wild type, fixed and embedded them for electron microscopy, and analyzed longitudinal sections with the use of image-averaging procedures (Mastronarde *et al.*, 1992; O'Toole *et al.*, 1995). Previous studies have shown that the I1 complex is a tri-lobed structure that occupies a specific position proximal to the first radial spoke and repeats every 96 nm along the length of the axoneme (Piperno *et al.*, 1990; Mastronarde *et al.*, 1992). Figure 2A shows an average from several wild-type axonemes. The relative positions of the radial spokes, the outer dynein arms, and the inner dynein arm structures are indicated in the model in Figure 2B. The I1 complex corresponds to lobes 1, 2, and 3; these structures are present in the wild-type axonemes (Figure 2A) but appear to be missing in the *ida2-6* axonemes (Figure 2C). The difference plot (Figure 2D) confirms that *ida2-6* axonemes lack the I1 structure and further demonstrates that this is the only significant difference between the *ida2-6* and wild-type images.

The I1 complex is composed of two Dhcs (1α and 1β), three ICs, and three LCs (Piperno *et al.*, 1990; Porter *et al.*, 1992; Harrison *et al.*, 1998). To ascertain whether all of the I1 complex polypeptides are missing in *ida2-6*, axonemes were isolated from wild type, *ida2-6*, and *pf9-2*, a previously characterized I1 mutant (Porter *et al.*, 1992), and analyzed by SDS-PAGE. In Figure 3A, the 1α and 1β Dhcs can be seen as

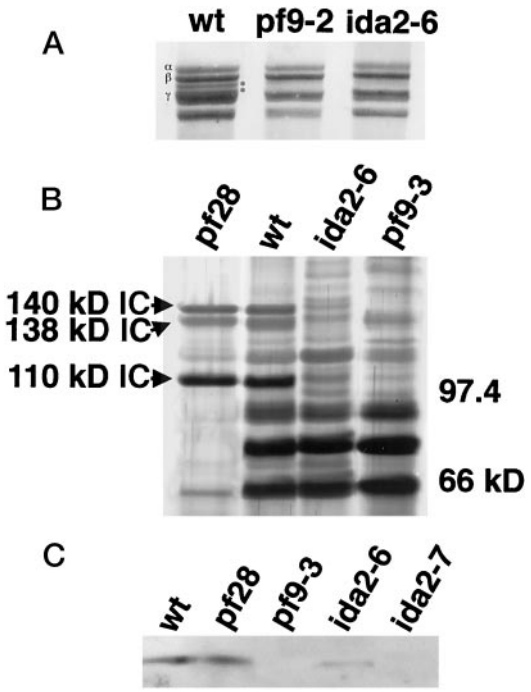

Figure 3. Dynein polypeptide defects in *ida2-6* axonemes. (A) The high-molecular-weight region of a 3–5% polyacrylamide, 3–8 M urea gradient gel that was loaded with whole axonemes from wild type, *pf9-2*, and *ida2-6* is shown here. The 1α and 1β Dhcs of the I1 complex, which migrate between the outer arm β and γ Dhcs, are indicated by the asterisks on the right. Both *pf9-2* and *ida2-6* lack the 1α and 1β Dhcs. (B) Sucrose density gradient centrifugation of dynein extracts from *pf28*, wild type, *ida2-6*, and *pf9-3*. All sucrose gradient fractions were loaded on 5–15% polyacrylamide gels. The subunits of the I1 complex sediment in the 18–19S region, along with contaminating outer arm components (Piperno *et al.*, 1990; Porter *et al.*, 1992). Only the 18–19S peaks are shown here. IC140, IC138, and IC110 are visible in *pf28* (which lacks the outer arm components) and wild type. (C) Western blot of wild-type and mutant axonemes probed with the antibody to the Tctex1 LC.

two faint bands migrating between the outer arm β and γ Dhcs in wild-type axonemes. Both the 1α and 1β Dhcs appear to be missing in the *pf9-2* and *ida2-6* axonemes. To examine the dynein ICs, crude dynein extracts from wild type, *ida2-6*, *pf9-2*, and the outer arm mutant *pf28* were fractionated by sucrose density gradient centrifugation and analyzed on 5–15% polyacrylamide gels. As shown in Figure 3B, the three ICs are clearly visible in the wild-type and *pf28* samples but appear to be missing or reduced in the *pf9-2* and *ida2-6* extracts. To analyze the dynein LCs, Western blots of whole axonemes were probed with an antibody specific for the 14-kDa LC, Tctex1, which is also one of the *t* haplotype gene products (Harrison *et al.*, 1998). Tctex1 was present in wild-type axonemes but appeared to be missing or reduced in the *ida2-6* sample (Figure 3C). Therefore, most of the I1 dynein subunits are not assembled into the *ida2-6* axonemes.

Cloning the IDA2 Locus

Because the *ida2-6* mutation was generated by plasmid insertion, we expected to see a deletion or rearrangement of *ida2-6* genomic DNA on Southern blots hybridized with the *Dhc10* sequence. However, we did not detect any obvious polymorphisms in *ida2-6* using the 150-bp PCR product as a probe. Therefore, to identify the gene that was disrupted in *ida2-6*, we recovered genomic DNA flanking the site of plasmid insertion. Southern blot analysis revealed that at least three copies of the *NIT1* plasmid had integrated into *ida2-6* genomic DNA, and all three copies cosegregated with the slow-swimming phenotype in the progeny (Figure 4A). Using the *NIT1* plasmid as a probe, we then identified a 3.4-kb *Kpn*I–*Cla*I restriction fragment in *ida2-6* that was likely to contain both plasmid sequence and flanking genomic DNA (see MATERIALS AND METHODS and Figure 4B). The 3.4-kb fragment was subsequently cloned by screening a size-fractionated mini library with the *NIT1* sequence and further characterized to identify a 350-bp *Kpn*I–*Sau*3A fragment containing only *ida2-6* genomic DNA. Southern blot analysis confirmed that this 350-bp fragment was derived from the region flanking the site of plasmid insertion in *ida2-6* (Figure 4C).

The 350-bp fragment was then used to screen a large-insert, wild-type genomic library, and seven overlapping phage clones spanning ~21.5 kb of genomic DNA were recovered (Figure 5, A and B). The library was also screened with the 150-bp PCR fragment of *Dhc10*, and four phage clones spanning ~27.8 kb of genomic DNA were recovered (Figure 5C). Comparison of the restriction maps and Southern blots probed with selected subclones confirmed that the two sets of clones overlapped.

To determine how the *Dhc10* gene was disrupted by the plasmid-insertion event in *ida2-6*, we used the phage clones to characterize both wild-type and mutant strains on Southern and Northern blots. Southern blots of wild-type and *ida2-6* genomic DNA were probed with selected subclones and analyzed for deletions and/or rearrangements within the *IDA2/Dhc10* region. The results are summarized in Figure 5A; all three copies of the *NIT1* plasmid in *ida2-6* were inserted into a region corresponding to the 4.7-kb *Sac*I fragment in wild type, ~6 kb upstream from the region encoding the first *Dhc10* phosphate-binding motif (P-loop). Surprisingly, this plasmid-insertion event was not accompanied by a large deletion of genomic DNA in *ida2-6*, which explained why we previously failed to see an RFLP with the 150-bp P-loop probe for *Dhc10*.

To investigate how many transcripts are present in the *IDA2/DHC10* region and how they might be altered in the *ida2-6* mutant, we isolated total RNA from wild type and *ida2-6* and analyzed the transcripts on Northern blots. Because flagellar transcripts are typically up-regulated in response to deflagellation, we isolated RNA both before and after deflagellation and then hybridized the Northern blots with subclones covering the cloned region. This analysis indicated that the *Dhc10* transcription unit spans ~25 kb of genomic DNA (Figure 5A) and encodes an ~13-kb transcript in wild-type whose expression is enhanced by deflagellation (Figure 4D). Moreover, when we used a probe located close to the site of plasmid insertion in *ida2-6*, it became apparent that the *Dhc10* transcript is significantly smaller (~4 kb) in the *ida2-6* mutant (Figure 4D). The plasmid insertion in *ida2-6*, therefore, disrupted the *Dhc10* transcription unit upstream of the region encoding the first P-loop (Figure 5A).

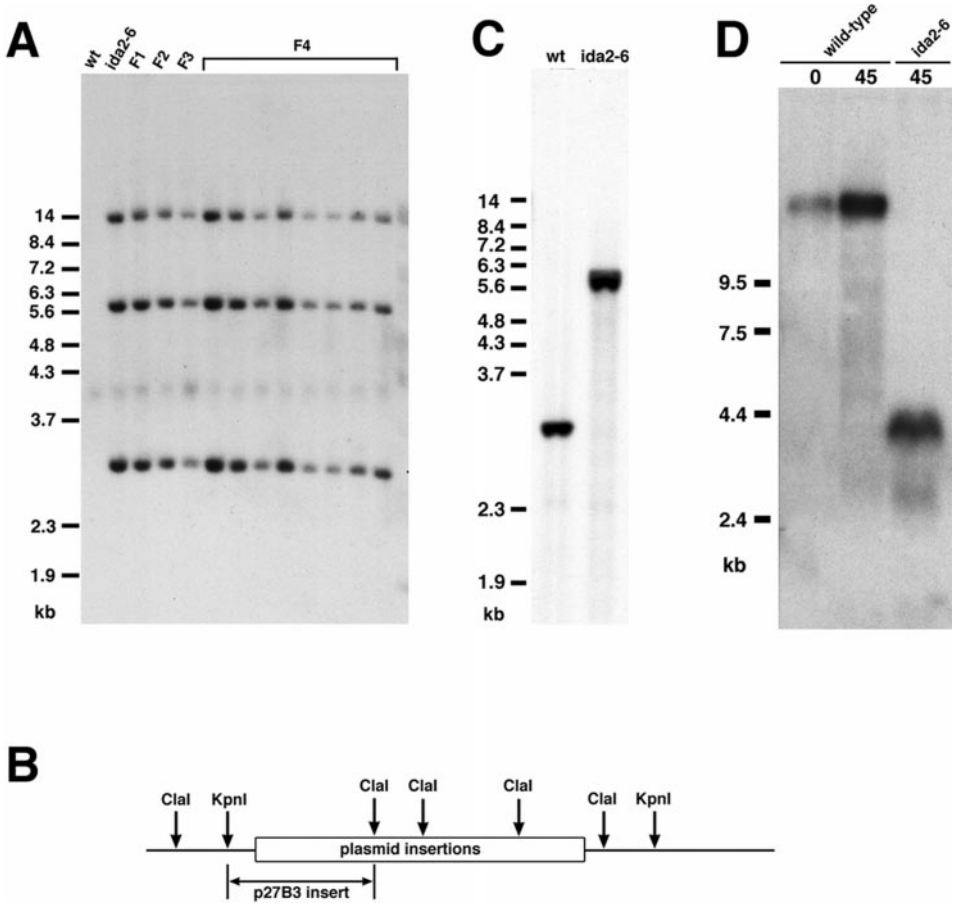

Figure 4. Recovery of genomic DNA flanking the site of the *ida2-6* mutation. (A) Cosegregation of plasmid sequences with the *ida2-6* motility defect. Shown here is an autoradiogram of a genomic Southern blot of *Sph*I-digested DNA from a wild-type strain, *ida2-6*, and the slow-swimming progeny from four successive generations (F1, F2, F3, and F4) of *ida2-6* × *nit1* crosses. The blot was hybridized with the vector sequence from the *NIT1* plasmid. Three copies of the plasmid are present in *ida2-6* and all of the slow-swimming progeny. (B) Diagram of the plasmid insertion in *ida2-6* and the strategy used to clone genomic DNA flanking the site of insertion. Genomic DNA from *ida2-6* was digested with *Cla*I, which cuts once per plasmid, and *Kpn*I, which does not cut within the plasmid sequences. Southern blots probed with the *NIT1* plasmid identified a unique 3.4-kb *Kpn*I–*Cla*I fragment in *ida2-6* containing genomic DNA adjacent to the inserted plasmids. This fragment was cloned from a size-fractionated mini library to yield the plasmid p27B3 (see MATERIALS AND METHODS). p27B3 was then digested with *Kpn*I–*Sau*3A to release a 350-bp fragment containing only genomic DNA. (C) Genomic Southern blot of wild-type and *ida2-6* DNA probed with the 350-bp *Kpn*I–*Sau*3A fragment. A RFLP is clearly visible between the two strains, confirming that the genomic DNA is close to the site of plasmid insertion in *ida2-6*. (D) Northern blot of wild-type and *ida2-6* RNA hybridized with a 3.2-kb *Sac*I fragment from the end of phage clone C. A single large (>13 kb) transcript is visible in wild type, and its expression is increased after deflagellation (compare 0 and 45 min). The *Dhc10* transcript is significantly smaller in *ida2-6* (~4 kb), but it is still expressed at a high level after deflagellation. This transcript also hybridizes with a *NIT8* probe (see text). To ensure that equal quantities of RNA were loaded in all lanes, Northern blots were also hybridized with the *CRY1* gene encoding the ribosomal S14 subunit.

Sequence Analysis of Dhc10

To further characterize the *Dhc10* gene and its encoded product, we sequenced the *Dhc10* transcription unit (EMBL accession numbers AJ242523–AJ242525). Putative exons were identified using codon preference programs and the conserved consensus sequences for *Chlamydomonas* splice donor and acceptor sites. All predicted splice sites were confirmed by sequence analysis of RT-PCR products (see MATERIALS AND METHODS). The predicted structure of the *Dhc10* transcription unit is shown in Figure 5F. It includes ~1 kb of sequence upstream from the proposed translation start site, ~24 kb of coding region containing 53 exons, and ~1.3 kb downstream from the proposed stop codon.

The deduced amino acid sequence of the *Dhc10* gene product is shown in Figure 6. It contains 4513 residues and corresponds to a polypeptide of 510,628 Da. Analysis of the predicted amino acid sequence with the GCG program Motifs revealed the presence of three P-loops that conform to the consensus sequence GXXXXGKT/S for a nucleotide-binding site (Walker *et al.*, 1982). A fourth P-loop that deviates from the consensus sequence (GVGGSGRK) was identified by alignment with other Dhc sequences. These four P-loops are spaced at ~300-amino acid intervals within the central region of the Dhc (Figure 6), similar to those found in other Dhcs (reviewed by Gibbons, 1995). Recent sequence analysis has suggested that all Dhc sequences may contain two additional degenerate ATP-binding sites in the C-terminal region (Neuwald *et al.*, 1999). Alignment with the cytoplasmic Dhc from *Dictyostelium* (Koonce et al., 1992) has confirmed that these sites are conserved in the *Dhc10* gene product (Figure 6).

To determine whether the *Dhc10* gene product contains the structural features seen in other Dhcs, we analyzed the deduced amino acid sequence using the COILS program (Lupus *et al.*, 1991; Lupus, 1996). This analysis (Figure 7) identified two regions with a high probability of forming α-helical coiled coils on either side of the central catalytic domain (residues 1535–1570 and 3088–3178), consistent with the structural predictions reported for other Dhcs (Mitchell and Brown, 1994, 1997). By analogy with other Dhc sequences, the C-terminal coiled-coil domains probably corre-

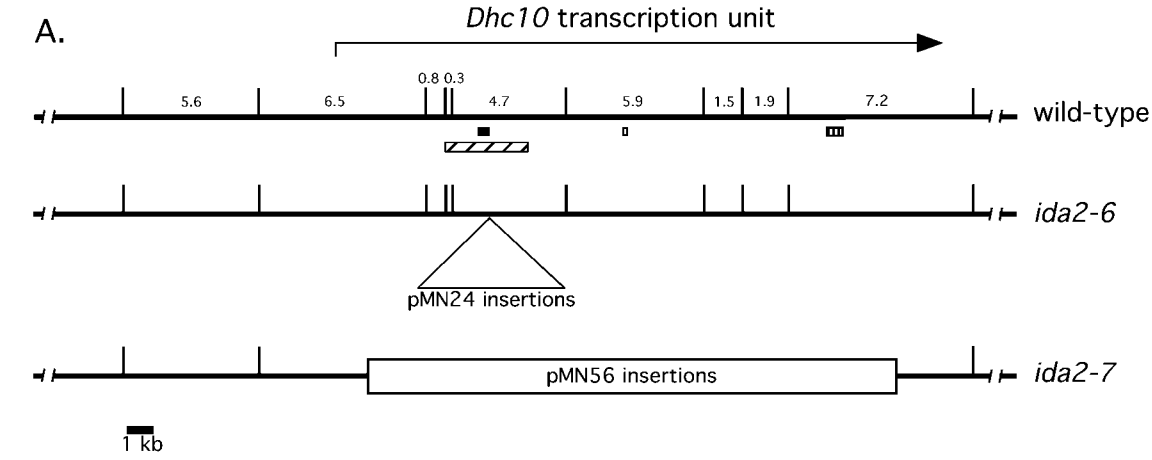
A.
Dhc10 transcription unit
0.8 0.3
5.6
6.5
4.7
5.9
1.5
1.9
7.2
wild-type
ida2-6
pMN24 insertions
pMN56 insertions
ida2-7
1 kb

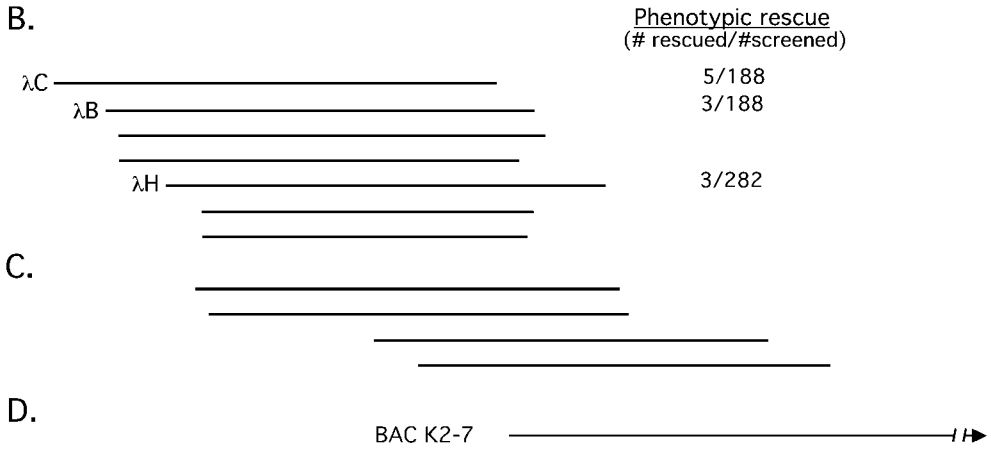
B.
Phenotypic rescue
(# rescued/#screened)
λC
5/188
λB
3/188
λH
3/282
C.
D.
BAC K2-7

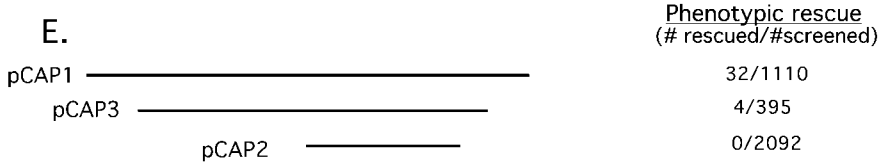
E.
Phenotypic rescue
(# rescued/#screened)
pCAP1
32/1110
pCAP3
4/395
pCAP2
0/2092

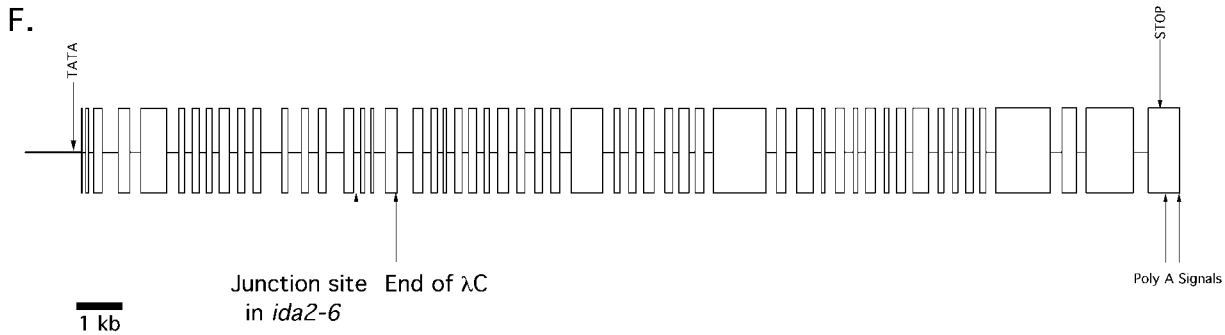
F.
TATA
STOP
Junction site
in *ida2-6*
End of λC
Poly A Signals
1 kb

spond to the stalk structure identified as the B-link (Goodenough *et al.*, 1987) and presumably contain the microtubule-binding site (Gee *et al.*, 1997; Koonce, 1997). The *Dhc10* gene product also contains a predicted coiled-coil domain close to the N terminus (residues 192–227); this domain appears to be unique to the *Dhc10* sequence.

Comparison of the predicted amino acid sequence of the *Dhc10* gene product with other axonemal Dhc sequences in *Chlamydomonas* indicates that they share significant sequence identity and similarity throughout their lengths. The greatest similarity is seen with the 1α Dhc of the I1 complex (34% identity and 62.6% similarity), and this homology extends into the N-terminal region (24% identity and 54.4% similarity within the first 1500 residues). Alignments with the programs Pileup and Clustal W have confirmed the presence of conserved domains within the N-terminal region but have also revealed several short stretches of sequence divergence. One of these regions, corresponding to residues 945–959 of the *Dhc10* gene product, was used to design a specific peptide epitope for antibody production (see MATERIALS AND METHODS). This region was also chosen because we were previously successful in obtaining a Dhc-specific antibody to the analogous region in the 1α Dhc sequence (Myster *et al.*, 1997).

Figure 5 (facing page). Recovery of the *IDA2/Dhc10* transcription unit. (A) Shown on the top is a partial restriction map of the *IDA2/Dhc10* genomic region in wild type. Shown below is a diagram of the genomic region in two different insertional mutants, *ida2-6* and *ida2-7*. Vertical marks indicate *Sac*I sites; the approximate sizes of the restriction fragments are also indicated. The shaded rectangle corresponds to the 350-bp *Kpn*I–*Sau*3A probe recovered as the genomic fragment flanking the site of plasmid insertion in *ida2-6*; the small open rectangle corresponds to the 150-bp *Dhc10* PCR product; and the rectangle with hash marks indicates the 3.2-kb *Sac*I fragment isolated from the end of phage clone C. The approximate location of the *Dhc10* transcription unit is illustrated by the arrow. The *ida2-6* mutation was generated by plasmid insertion into the *Dhc10* coding region. The plasmid insertion event in *ida2-7* was associated with a large (>20 kb) deletion of the *Dhc10* transcription unit. (B) Wild-type phage clones recovered using the 350-bp *Kpn*I–*Sau*3A probe are shown with respect to the genomic region above. Clones C, B, and H were tested for their ability to rescue the motility defect of *ida2-6* by cotransformation. Clone C encodes up to residue 989 of the 1β Dhc sequence, and clone H encodes up to residue 1695. The resulting N-terminal fragments are predicted to have molecular masses of ~113 and 195 kDa, respectively, and completely lack the dynein motor domain. (C) Phage clones recovered using the 150-bp *Dhc10* PCR fragment. (D) A BAC clone that was recovered using an RT-PCR product from the 3′ end of the *Dhc10* gene. (E) Diagram of smaller subclones used in cotransformation experiments to rescue *ida2-6* and *ida2-7*. These subclones are drawn to scale with respect to parts A–D. pCAP1 encodes up to residue 989 of the 1β Dhc; pCAP2 encodes up to residue 508; and pCAP3 encodes up to residue 811. (F) Diagram of the intron/exon structure of the *Dhc10* gene as determined by RT-PCR. The exons are indicated by the open rectangles, and the introns are indicated by solid lines. A TATA box sequence located ~140 bp upstream of the proposed translation start site is also shown. The identification of the translation start site was based on the recovery of an RT-PCR product using a forward primer downstream of the TATA box sequence and a reverse primer from exon 3. This RT-PCR product contained stop codons in all three frames preceding the proposed start codon. The region upstream of the TATA box sequence also contains six tub box sequences thought to enhance the expression of flagellar genes (Davies and Grossman, 1994). The 3′ end of the gene is contained within the 7.2-kb *Sac*I subclone (see A). Two putative polyadenylation signals (TGTAA) were identified 116 and 445 bp downstream of the proposed stop site. Also shown are the sites that correspond to the junction between *Dhc10* and the plasmid insertions in *ida2-6*, and the 3′ end of the *Dhc10* sequence in phage clone C and pCAP1. The scale of this diagram is enlarged relative to parts A–E.

Dhc10 Encodes the 1β Dhc of the I1 Complex

Characterization of the affinity-purified *Dhc10* peptide antibody by Western blotting (Figure 8A) shows that *Dhc10* encodes the 1β Dhc of the I1 complex. The *Dhc10* antibody recognizes a Dhc present in wild-type and outer arm mutant axonemes but absent in I1 mutant axonemes (Figure 8B). To determine if the *Dhc10* antibody is specific for one of the two I1 Dhcs, we analyzed purified I1 dynein complexes on 5% polyacrylamide gels to resolve the 1α and 1β Dhcs. Duplicate immunoblots of the I1 complex were then probed with affinity-purified *Dhc1* and *Dhc10* antibodies. As shown in Figure 8A, the *Dhc1* antibody recognizes only with the 1α Dhc, as described previously (Myster *et al.*, 1997), whereas the *Dhc10* antibody recognizes only with the 1β Dhc. These results demonstrate that *Dhc10* is the structural gene for the 1β Dhc and that defects in the 1β Dhc are the basis of the *ida2* mutant phenotype.

ida2-6 Encodes a Truncated 1β Dhc Fusion Protein That Inhibits I1 Complex Assembly

The Northern blot shown in Figure 4D revealed that the *ida2-6* mutant generates a stable but truncated *Dhc10* transcript. This observation raised the possibility that the 1β Dhc fragment in *ida2-6* might lack a critical domain required for I1 complex assembly. To determine the nature of the truncated transcript in *ida2-6*, we sequenced the plasmid containing the junction between the *Dhc10* gene and the inserted pMN24 sequences (Figure 4B). This sequence revealed that the *Dhc10* gene is disrupted in intron 15 (Figure 5F) by the insertion of 63 bp of vector followed by a sequence that corresponds to the 3′ end of the *NIT8* gene present in the pMN24 plasmid (Zhang, 1996). The junction between the vector and the 3′ end of the *NIT8* gene forms a splice acceptor sequence, which could generate a transcript that fuses the 5′ end of *Dhc10* in-frame with the 3′ end of *NIT8*. Hybridization of the Northern blot shown in Figure 4D with the *NIT8* sequence has confirmed the presence of the hybrid transcript in *ida2-6*. The *ida2-6* gene product, therefore, is a fusion protein containing the first 827 residues (~94 kDa) of the 1β Dhc fused to the last 132 residues of the *NIT8* gene product.

Previous work on the expression of other Dhc sequences has indicated that N-terminal fragments between 140 and 160 kDa are capable of complex assembly (Sakakibara *et al.*, 1993; Koonce and Knecht, 1998; Iyadurai *et al.*, 1999; Myster *et al.*, 1999). Therefore, it was unclear whether the *ida2-6* mutation prevents the assembly of the I1 complex into the axoneme because the mutant 1β Dhc fragment lacks a specific domain required for dynein complex formation or because the *NIT8* sequence at the end of the 1β Dhc fragment destabilizes the complex. Comparison with another *ida2* mutant has now indicated that the 1β Dhc in *ida2-6* may retain some partial activity. Southern and Northern blot analysis of the *ida2-7* mutant has shown that the *Dhc10* transcription

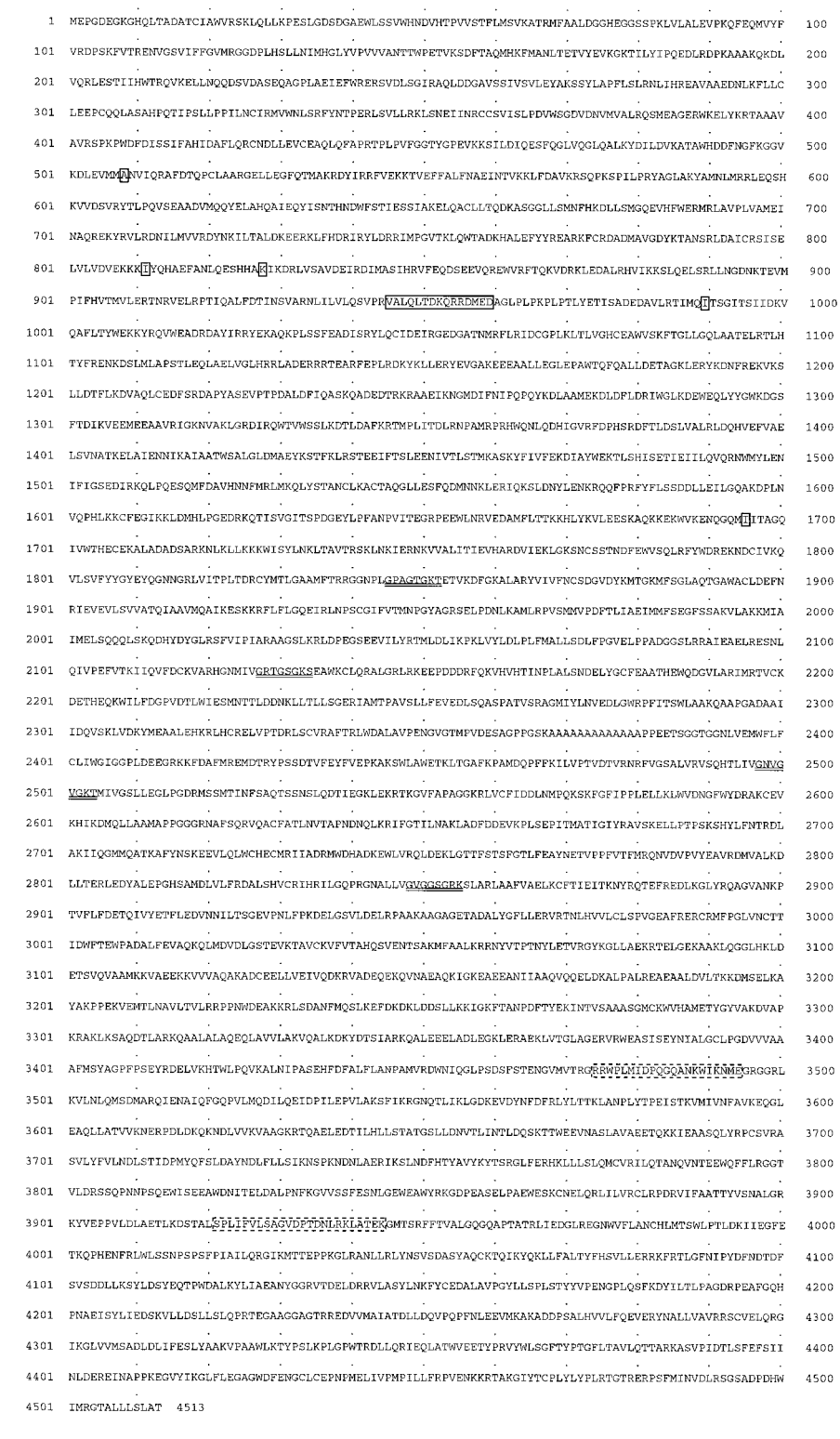

Figure 6. Predicted amino acid sequence of the 1β Dhc. The deduced amino acid sequence (residues 1–4513) of the *Dhc10* gene product is shown here. The four regions corresponding to P-loops 1–4 are underlined. The regions containing the degenerate P-loops identified by comparison with the cytoplasmic Dhc from *Dictyostelium* (Neuwald *et al.*, 1999) are indicated by the dashed boxes. The peptide sequence (VALQTDKQRRDMED) used to generate a specific antibody (residues 945–959) and the C-terminal amino acid residues encoded by the different *Dhc10* constructs used for cotransformation are also shown.

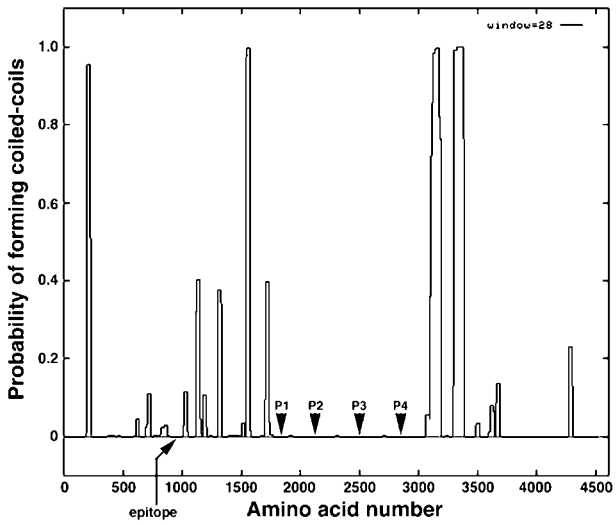

Figure 7. Diagram depicting regions of high coiled-coil probability for the *Dhc10* gene product. The plot was generated using the COILS program (Lupus *et al.*, 1991; Lupus 1996) with a window size of 28 and the MTIDK matrix. The approximate positions of the four central P-loops are indicated by the arrowheads.

unit is completely deleted in this strain (Figure 5A), and interestingly, its motility defect is even greater than that observed in *ida2-6* (Table 1). Moreover, when isolated axonemes from the two *ida2* mutants are compared on Western blots with the use of chemiluminescent detection procedures, small but detectable amounts of I1 complex polypeptides can be seen in the *ida2-6* axonemes but not in the *ida2-7* axonemes (Figure 8B). These results suggest that the 1β Dhc fragment in *ida2-6* can assemble into an I1 complex, but the mutant I1 complex is unstable and cannot assemble efficiently into the flagellar axoneme.

Partial Rescue of ida2 by Transformation with Dhc10 Constructs Encoding 1β Dhc Fragments

To identify the 1β Dhc domains required for I1 complex assembly, we crossed the *ida2* strains into an *arg7* mutant background and then cotransformed the double mutants with several of the clones shown in Figure 5 and the selectable marker *ARG7*. Arg+ transformants were then picked and screened for rescue of the *ida2* motility defect by light microscopy.

With each phage clone tested (Figure 5B), we recovered several cotransformants that appeared to swim more quickly than the original *ida2-6* mutant. The rescued cotransformants also regained the ability to phototax (Table 1). However, when we measured the swimming velocities of the rescued strains, it was clear that the motility phenotypes of the rescued cotransformants were not completely wild type. For example, the swimming velocity of the rescued *ida2-6* strain D11, which was cotransformed with phage clone C, was significantly faster than that of *ida2-6* (107.9 $\pm$ 15.3 μm/s versus 77.6 $\pm$ 15.4 μm/s) but still slower than that of wild type (144.2 $\pm$ 17.1 μm/s). This partial rescue of the motility defects would be consistent with the reassembly of a modified I1 complex lacking one of the two Dhc motor domains. Therefore, we sequenced the ends of the rescuing phage clones to determine the sizes of the predicted 1β Dhc fragments (Figure 5B). We also subcloned the rescuing DNA and tested progressively smaller *Dhc10* constructs for their ability to rescue the *ida2* motility defects (Figure 5E). Sub-

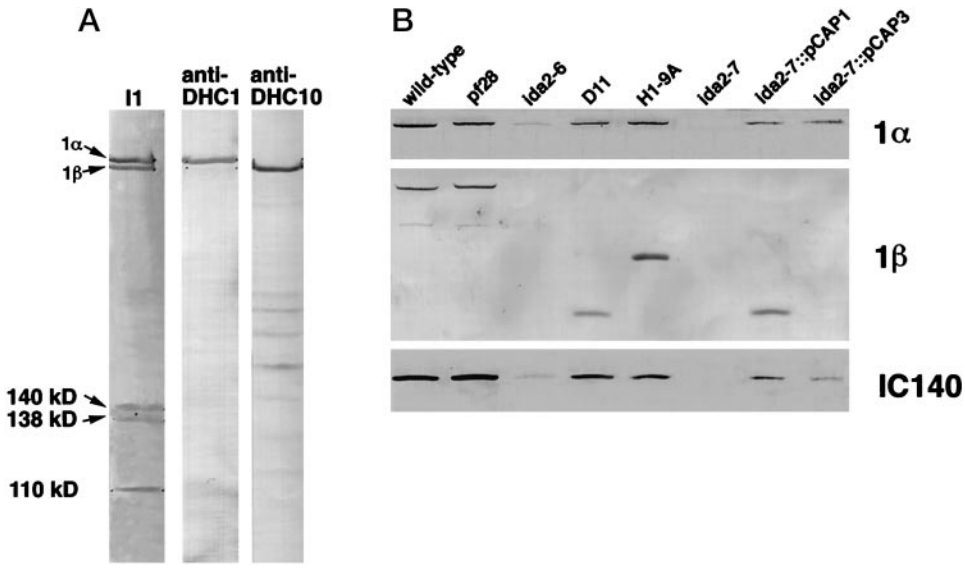

Figure 8. The *Dhc10* antibody identifies the 1β Dhc as the gene product of the *IDA2/Dhc10* locus. (A) Specificity of I1 Dhc antibodies. The I1 complex was purified by sucrose density gradient centrifugation and analyzed on 5% polyacrylamide gels to resolve the 1α and 1β Dhcs (left lane). Duplicate immunoblots were probed with an affinity-purified *Dhc1* antibody (middle lane) and an affinity-purified *Dhc10* antibody (right lane). (B) Reassembly of I1 complex subunits in *Dhc10* transformants. Axonemes were isolated from wild-type and mutant strains, run on 5% polyacrylamide gels, and blotted to either nitrocellulose or polyvinylidene difluoride. One strip containing only the Dhc region was probed with the *Dhc1* antibody to detect the 1α Dhc (top blot). A second strip containing the region above 85 kDa was probed with the *Dhc10* antibody to detect the 1β Dhc and related N-terminal fragments (middle blot). A third strip containing the 140-kDa region was probed with the IC140 antibody (bottom blot). *ida2-6* and *ida2-7* are two different insertional mutants (see Figure 5A). Both strains were cotransformed with *Dhc10* constructs encoding N-terminal 1β Dhc fragments of varying lengths (see Figure 5, B and E). Note that the 1β Dhc fragment encoded by the pCAP3 subclone does not contain the peptide epitope used to generate the *Dhc10* antibody, so the ~92-kDa fragment cannot be detected by Western blot analysis of axoneme polypeptides.

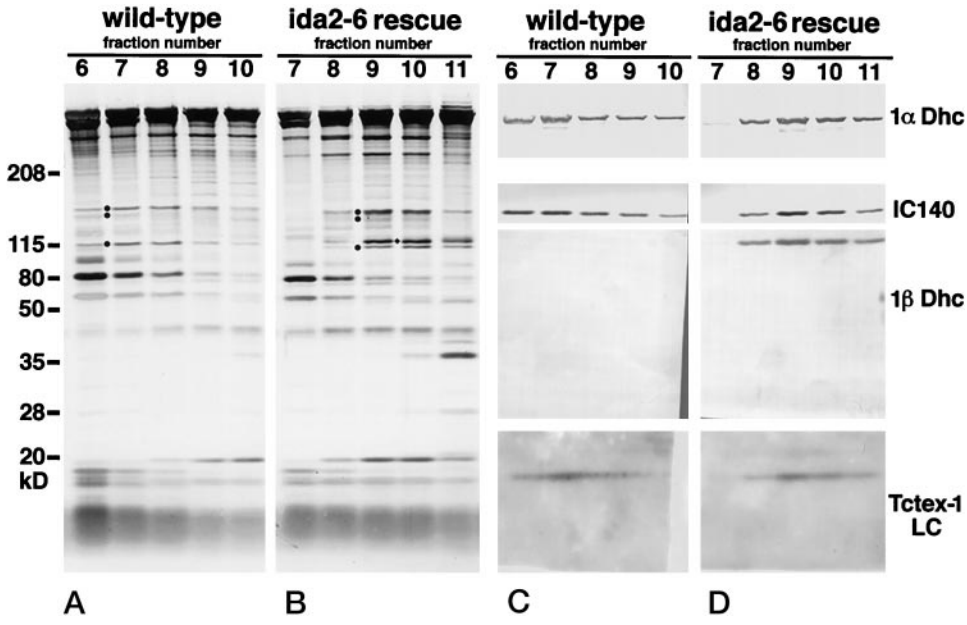

Figure 9. Formation of an I1 complex in the rescued *ida2* strain. Dynein extracts from wild type and the rescued *ida2-6* strain, D11, were subjected to sucrose density gradient centrifugation. The resulting fractions were run on duplicate 5–15% polyacrylamide gradient gels, and the gels were either silver stained or transferred to Western blots. (A) Gel of wild-type fractions sedimenting in the 19S region. The 110-, 138-, and 140-kDa ICs of the I1 complex (indicated by the solid circles) cosediment in fractions 6 and 7. (B) Gel of the rescued *ida2-6* strain, D11. The I1 ICs cosediment at 16S in fractions 9 and 10. A novel polypeptide migrating at ~113 kDa in fractions 9 and 10 is indicated by a diamond. This polypeptide is not present in the wild-type gradient. (C) Blots of the wild-type fractions shown in A were probed with antibodies against the 1α Dhc (top panel), IC140 (second panel), 1β Dhc (third panel), and Tctex1 LC (bottom panel). (D) Blots of the rescued *ida2-6* fractions shown in B were probed with I1 complex antibodies as described in C. Note the presence of the 1β Dhc fragment at ~113 kDa.

clones pCAP1 and pCAP3, encoding 989 and 811 residues, respectively, could partially rescue the motility defects of the *ida2* strains (Table 1), whereas subclone pCAP2, encoding only 508 residues, could not (Figure 5E). These results indicate that the region of the 1β Dhc between residues 508 and 811 is critical for I1 complex assembly and recovery of motility.

To verify that the *Dhc10* constructs encode functional 1β Dhc fragments, axonemes were isolated from several of the rescued transformants and analyzed on Western blots probed with I1 complex antibodies (Figure 8B). Immunoblots probed with the *Dhc10*-specific antibody demonstrated that the axonemes from the rescued strains did contain 1β Dhc fragments of the expected sizes (see Figure 8 legend). Probing the immunoblots with antibodies to other I1 complex subunits also showed that other components of the complex had been restored. Given that none of the *Dhc10* constructs tested encoded the 1β Dhc motor domain, we reasoned that the increased motility of the rescued strains must be due to the assembly of a modified I1 complex containing an N-terminal fragment of the 1β Dhc and a full-length 1α Dhc with an active motor domain.

To directly demonstrate the reassembly of the 1β Dhc fragment into an I1 complex, we prepared crude dynein extracts from wild type and one of the rescued *ida2-6* strains and then fractionated the extracts by sucrose density gradient centrifugation. All of the gradient fractions were analyzed on 5–15% polyacrylamide gradient gels and duplicate immunoblots. Figure 9 shows the fractions that contain I1 complex subunits in both wild type and the rescued *ida2-6* strain, D11. IC140, IC138, and IC110 are clearly visible at 18–19S in fractions 6 and 7 of the wild-type extracts (Figure 9A). However, in the rescued *ida2-6* extracts, the three ICs cosediment at 16S, in fractions 8–10, indicating that the sedimentation behavior of the I1 complex has been altered (Figure 9B). In addition, a novel band migrating just above IC110 cosediments with the I1 subunits in the rescued *ida2-6* extracts (Figure 9B). The size of this novel band is consistent with the predicted size of the truncated 1β Dhc fragment (~113 kDa) seen in the rescued strain (Figure 8B). Duplicate immunoblots of these fractions probed with antibodies against the 1α Dhc, 1β Dhc, IC140, and Tctex1 demonstrate that all of the I1 subunits cosediment at 18–19S in wild-type extracts (Figure 9C) and at 16S in the rescued *ida2-6* extracts (Figure 9D). Furthermore, the novel band seen at ~113 kDa in the rescued strain is recognized by the *Dhc10*-specific antibody, confirming the presence of the N-terminal 1β Dhc fragment in the modified I1 complex.

Localization of the 1β Motor Domain within the I1 Structure

To explore the effect of the truncated 1β Dhc on the structure of the I1 complex, we isolated axonemes from the rescued *ida2-6* strain, fixed and embedded them for electron microscopy, and analyzed longitudinal thin sections using image-averaging procedures (O'Toole *et al.*, 1995). As shown in Figure 2E, the average of the rescued *ida2-6* axonemes indicates that densities of the I1 complex have been partially restored. The details can be seen more easily in the difference plot between wild-type and rescued *ida2-6* axonemes (Figure 2F). The structures represented by lobes 2 and 3 have reappeared in the rescued strain, but lobe 1 is still missing. A small loss of density is also seen extending from lobe 1 to lobe 3. These results suggest that the central and C-terminal 75% of the 1β Dhc, which corresponds to the missing motor domain in the mutant, forms the globular head domain located in lobe 1. Furthermore, because lobe 2 has been identified as the site of the 1α Dhc motor domain (Myster *et al.*, 1999), we conclude that lobe 3 is the site of the N-terminal

regions of the Dhc and the associated IC and LC subunits of the I1 complex.

DISCUSSION

The IDA2 Locus Corresponds to a Dhc Gene Required for Flagellar Motility

In previous work, we identified a large family of *Dhc* genes in *Chlamydomonas* whose expression patterns were consistent with a role in axoneme assembly or motility (Porter *et al.*, 1996, 1999). In this report, we now demonstrate that one of these genes, *Dhc10*, maps to the *IDA2* locus (Figure 1) and plays an essential role in the assembly and activity of the I1 inner arm complex. Disruption of the *Dhc10* gene by plasmid insertion (Figure 5) resulted in the formation of a truncated transcript (Figure 4) whose encoded gene product reduces the assembly of the I1 complex into a flagellar axoneme (Figures 2 and 3), leading to defects in the flagellar waveform, forward swimming velocity, and phototaxis (Table 1).

Sequence Analysis of the Dhc10 Transcription Unit

Dhc10 encodes a polypeptide that is very similar to other *Chlamydomonas* axonemal Dhcs (Mitchell and Brown, 1994; Wilkerson *et al.*, 1994; Myster *et al.*, 1999). For example, the central region of the polypeptide is bounded on both sides by regions predicted to form coiled-coil domains (Figure 7), and it also contains multiple P-loop sequences spaced at intervals similar to those observed in other Dhc sequences (Figure 6). The first P-loop is 100% identical to those found in other axonemal Dhcs, whereas the second and third P-loops are less well conserved. The fourth P-loop deviates from the consensus sequence found in other axonemal Dhcs (GVGGSGKQ) in that the terminal lysine and glutamine residues are replaced by an arginine and a lysine, respectively (GVGGSGRK). Two degenerate P-loop–like repeats were also found downstream from the C-terminal coiled-coil domain (Figure 6), as described previously for the cytoplasmic Dhc (Neuwald *et al.*, 1999). Comparisons with *Dhc* genes identified in other organisms (Figure 1) have identified homologues of the *Dhc10* sequence in sea urchin (*TgDhc5C*), rat (*Dhc2*), mouse (*Dhc5*), and *Paramecium* (*Dhc5*). The *Dhc10*-related transcripts appear to be most abundant in ciliated cells and tissues (Tanaka *et al.*, 1995) and/or up-regulated in response to deciliation (Gibbons *et al.*, 1994). Thus, it is likely that the *Dhc10*-related genes encode polypeptide sequences required for axonemal motility in these organisms as well.

The Dhc10 Gene Encodes the 1β Dhc of the I1 Complex

Several lines of evidence indicate that *Dhc10* encodes the 1β Dhc of the I1 complex. First, the disruption of the *Dhc10* gene in *ida2-6* results in the failure to assemble the I1 complex (Figures 2, 3, and 5), which is composed of two Dhcs (1α and 1β), and associated ICs and LCs (Piperno *et al.*, 1990; Porter *et al.*, 1992; Harrison *et al.*, 1998). Although defects in either the 1α or 1β Dhc might be predicted to result in an I1 mutant phenotype, we have shown previously that the 1α Dhc is encoded by a different *Dhc* locus (Myster *et al.*, 1997). Second, amino acid sequence comparisons between axonemal Dhcs indicate that the *Dhc10* gene product is most similar to the 1α Dhc (Myster *et al.*, 1999), as might be expected for two Dhcs that coassemble into a heteromeric dynein complex. Finally, the generation of *Dhc10*-specific antibody that exclusively recognizes the 1β Dhc subunit in wild-type strains and related N-terminal fragments in the *Dhc10* transformants (Figure 8) clearly establishes that the 1β Dhc is the *Dhc10* gene product.

Rescue of ida2 Mutants with Truncated Dhc10 Genes: Implications for Assembly Domains within Dhcs

We have been able to partially rescue the motility defects in *ida2* mutants by transformation with truncated *Dhc10* genes. Our results indicate that the rescue is due to the reassembly of a modified I1 complex containing a full-length 1α Dhc and a truncated 1β Dhc that lacks the motor domain (Table 1, Figures 2, 9, and 10). Although the assembly of dynein complexes with N-terminal fragments has been described (Sakakibara *et al.*, 1993; Iyadurai *et al.*, 1999; Myster *et al.*, 1999), all of those fragments were considerably larger (140–160 kDa) than those reported here. We have found that a 92-kDa N-terminal fragment containing 811 residues of the 1β Dhc, or <20% of the full-length Dhc, can still support the formation of the I1 complex, its transport to the flagellar compartment, and its assembly onto the flagellar axoneme, but fragments containing only 508 residues cannot (Figures 5 and 10A). These results indicate that the region between residues 508 and 811 contains a critical domain required for complex assembly. Interestingly, Clustal W alignment of Dhc sequences has shown that this region is moderately well conserved between both axonemal and cytoplasmic Dhc sequences. In addition, the assembly domain of the 1β Dhc overlaps with the region identified in the *Dictyostelium* cytoplasmic Dhc as critical for subunit association in vitro (Habura *et al.*, 1999). Together, these observations suggest that the limited sequence homologies observed between the N-terminal regions of the cytoplasmic and axonemal Dhcs are related to their similar roles in the subunit interactions that lead to dynein complex assembly.

Contribution of the 1β Dhc Motor Domain to Motility and Phototaxis

Partial rescue of the *ida2* motility defects was observed with *Dhc10* constructs that completely lack the region encoding the 1β Dhc motor domain, and the swimming velocities of the rescued strains were intermediate between that of wild type and that of the particular *ida2* mutant used as host (Table 1). A similar reduction in swimming velocity was also seen in strains that lack the 1α motor domain (Myster *et al.*, 1999). We interpret the reduced swimming velocities relative to wild type as a direct effect of the loss of one of the two I1 Dhc motor domains. However, it is also interesting to compare the maximal speed of the *Dhc10* rescued strains, which swim forward at ~108 μm/s, with that of the *Dhc1* transformants, which swim forward at ~137 μm/s (Table 1) (Myster *et al.*, 1999). These differences imply that the contribution of the 1β Dhc motor domain to forward swimming velocity is greater than that of the 1α Dhc. In addition, these results suggest that the two dynein heads can function as independent motor units and that the loss of one head does

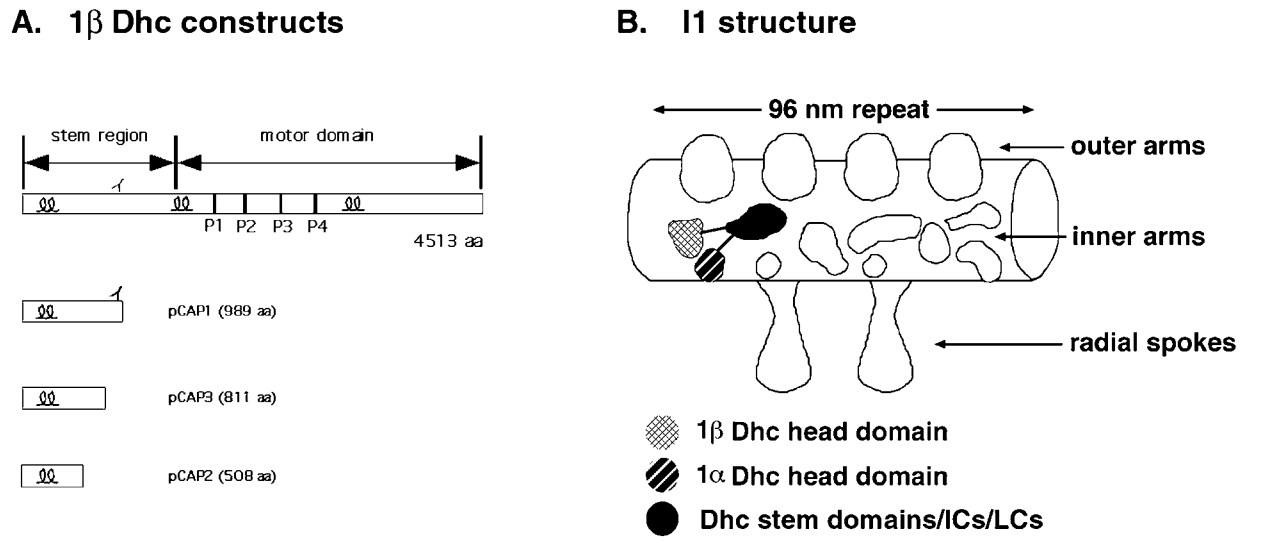

Figure 10. (A) Scheme of 1β Dhc and N-terminal fragments analyzed in this study. Also indicated are the locations of the P-loops (P1, P2, P3, and P4) and the regions predicted to form α-helical coiled coils (curlicues). (B) Scheme illustrating the location of I1 complex components within the structure of the 96-nm axoneme repeat.

not inhibit the activity of the second motor domain. This differs from the results described previously for cytoplasmic dynein (Iyadurai *et al.*, 1999).

Transformation of *ida2* strains with truncated *Dhc10* constructs not only resulted in an increased swimming velocity but also rescued the ability of the mutants to phototax. Given that strains lacking only the 1α head domain can also phototax in the presence of outer arms (Myster *et al.*, 1999), it appears that only one I1 Dhc motor domain is necessary for a normal phototactic response. However, it is also possible that the rescued phenotype is not due directly to the dynein motor domain but instead is due to the reassembly of the associated IC/LC complex into the axoneme. For example, IC138 has been identified previously as an important component in the phototaxis response, because strains with altered IC138 phosphorylation states are unable to phototax (King and Dutcher, 1997). Clearly, additional work is needed to understand how the phosphorylation state of IC138 alters the activity of the I1 dynein motor domains during the phototaxis response.

Implications for the Structure, Assembly, and Regulation of the I1 Complex

Electron microscopic analysis of axonemes from the rescued strains has allowed us to determine the structural defects associated with the assembly of an I1 complex lacking the 1β motor domain. As shown in Figure 2, E and F, lobes 2 and 3 of the I1 complex are largely restored in axonemes obtained from the rescued strain. The major defect associated with the missing 1β motor domain is the loss of lobe 1, although some loss of density can also be seen extending into lobe 3. Structural analysis of strains lacking the 1α motor domain has identified similar defects in lobe 2 (Myster *et al.*, 1999). Combining these data, we can now infer that lobe 3 of the I1 structure contains the N-terminal regions of the two Dhcs as well as the associated IC/LC complex (Figure 10B).

These observations have important implications for both the assembly and the regulation of the I1 complex. Previous work has indicated that both IC140 and IC110 play structural roles in the assembly of the I1 complex and its binding to the A-tubule of the flagellar axoneme (Perrone *et al.*, 1998; Yang and Sale, 1998). The localization of IC140 and IC110 to lobe 3 confirms that lobe 3 is the site for the attachment of the I1 complex to the outer doublet microtubule. These findings are also consistent with views of this region in axoneme cross-sections (Mastronarde *et al.*, 1992). In vitro reconstitution studies have further shown that both purified I1 complexes and expressed fragments of IC140 can rebind specifically to vacant sites in I1 mutant axonemes, but they will not bind to wild-type axonemes or purified tubulin (Smith and Sale, 1992; Yang and Sale, 1998). These results suggest the presence of accessory proteins that function as docking structures for the attachment of the I1 complex, similar to that observed in the outer dynein arm (Takada and Kamiya, 1994). Such docking proteins must be located in close proximity to lobe 3.

The association of IC138 with the base of the I1 complex is also significant in light of its proposed role in regulating dynein arm activity. As described above, mutations that affect the phosphorylation state of IC138 result in the loss of the ability to phototax (King and Dutcher, 1997). Furthermore, increases in microtubule sliding velocities in response to signals from the radial spokes are associated with changes in the phosphorylation state of IC138 (Habermacher and Sale, 1997), and both an axonemal phosphatase and an axonemal kinase appear to be involved (Yang and Sale, 1999; Yang *et al.*, 2000). The localization of IC138 to lobe 3 places IC138 in relatively close proximity to the first radial spoke, which would be an ideal location for a component that mediates signals between the radial spokes, axonemal kinases or phosphatases, and the dynein motor domains. The

axonemal kinases and phosphatases that act on IC138 also must be located near lobe 3.

The I1 complex LCs are also located in lobe 3, at the base of the I1 structure. Western blots of I1 complexes lacking one or the other Dhc motor domain reveal wild-type levels of the 14-kDa Tctex1 LC (Figure 9). Similar results have been seen with antibodies against the 8-kDa LC (our unpublished results). Together with other studies, these findings suggest that the 8-kDa LC plays multiple roles in the assembly and transport of the I1 complex. It may function to stabilize the I1 dynein and other dyneins containing multiple Dhcs during complex formation (Benashski *et al.*, 1997; Harrison *et al.*, 1998), and it may interact with the transport machinery involved in flagellar assembly (Cole *et al.*, 1998). It is clearly required for the retrograde transport of components during flagellar assembly and maintenance, presumably as a subunit of a cytoplasmic dynein motor (Pazour *et al.*, 1998).

The localization of Tctex1 to the base of the I1 complex is significant in light of its proposed role in the targeting of dynein complexes to specific cellular locations or cargoes (Harrison *et al.*, 1998; King *et al.* 1998; Nagano *et al.*, 1998; Tai *et al.*, 1998, 1999). For instance, Tctex1 may serve to direct the I1 complex to its specific location in the 96-nm axoneme repeat (Figure 10B). Tctex1 is also known to bind directly to the *fyn* protein kinase in vitro (Campbell *et al.*, 1998). These results and its position at the base of the I1 complex suggest that it may also facilitate interactions with the axonemal kinases that modify the activity of the I1 complex in situ (Habermacher and Sale, 1997; King and Dutcher, 1997).

The position of the Tctex1 LC may also be important with respect to its proposed function as one of the distorter gene products of the mouse *t* complex (Lader *et al.*, 1989; Harrison *et al.*, 1998). The *t* complex is a region of mouse chromosome 17 containing several genes that affect sperm motility and male fertility. Mutations in the *t* haplotype are usually inherited as a single group in a nonmendelian manner (reviewed by Silver, 1993; Olds-Clarke, 1997), and genetic analyses have indicated that this nonmendelian inheritance is the result of the interaction of several distorter gene products with a single responder gene product (Lyon, 1984, 1986). After the identification of Tctex1 and the outer arm LC, Tctex2, as two candidates for the distorter gene products, Patel-King *et al.* (1997) proposed a model in which the responder might function as a gatekeeper during flagellar assembly that interacts directly with the LCs and affects sperm motility. Mutations in the Tctex LCs would poison the *wt*-bearing sperm associated with a wild-type responder by the incorporation of defective dynein complexes that reduce sperm motility (Patel-King *et al.*, 1997; Harrison *et al.*, 1998). However, *t*-bearing sperm with a mutant responder would interact preferentially with wild-type dynein complexes, with the result that *t*-bearing sperm would be more motile than *wt*-bearing sperm (Patel-King *et al.*, 1997; Harrison *et al.*, 1998). The recent discovery that the *t* complex responder is a mutant form of a testis-specific, sperm motility kinase (smok) (Herrmann *et al.*, 1999) suggests that defects in the phosphorylation of dynein subunits could be the basis of the *t* complex phenotype. Indeed, changes in the phosphorylation state of the Tctex LCs have been correlated with changes in sperm motility in other species (Inaba *et al.*, 1999). Determining the subcellular distribution of *smok* kinase and its position relative to the Tctex1 and Tctex2 dynein LCs is clearly the next step needed to understand how these components interact to regulate flagellar motility.

ACKNOWLEDGMENTS

We thank other members of the Porter laboratory for their support and advice during the course of this project, especially Katrina Wysocki for technical assistance with the sequence analysis of the 3′ end of the *Dhc10* gene and the phenotypic analysis of *Dhc10* transformants. We are also grateful to the members of the laboratories of Carolyn Silflow, Pete Lefebvre, and Dick Linck for their helpful suggestions during our weekly group meetings, and to Tom Hays for his thoughtful comments on the manuscript. We extend a special thanks to Rogene Schnell for her suggestions on the recovery of flanking DNA from the 27B3 strain. Win Sale (Emory University) and Steve King (University of Connecticut) generously provided antisera for IC140 and Tctex1, respectively. Parts of this work were completed by C.A.P. in partial fulfillment of the requirements for a Ph.D. degree at the University of Minnesota. This work was supported by a grant from the National Institutes of General Medical Sciences (GM 55667) to M.E.P. C.A.P. was supported in part by a research training grant from the National Science Foundation for Interdisciplinary Studies on the Cytoskeleton (DIR9113444). E.T.O. was supported by a National Institutes of Health Biotechnology Resource grant (RR00592) to J.R. McIntosh.

REFERENCES

Benashski, S.E., Harrison, A., Patel-King, R.S., and King, S.M. (1997). Dimerization of the highly conserved light chain shared by dynein and myosin V. J. Biol. Chem. *272*, 20929–20935.

Campbell, K.S., Cooper, S., Dessing, M., Yates, S., and Buder, A. (1998). Interaction of $p59^{fyn}$ kinase with the dynein light chain, Tctex1, and colocalization during cytokinesis. J. Immunol. *161*, 1728–1737.

Cole, D.G., Diener, D.R., Himelblau, A.L., Beech, P.L., Fuster, J.C., and Rosenbaum, J.L. (1998). *Chlamydomonas* kinesin-II-dependent intraflagellar transport (IFT): IFT particles contain proteins required for ciliary assembly in *Caenorhabditis elegans* sensory neurons. J. Cell Biol. *141*, 993–1008.

Davies, J.P., and Grossman, A.R. (1994). Sequences controlling transcription of the *Chlamydomonas reinhardtii* β_2-tubulin gene after deflagellation and during the cell cycle. Mol. Cell. Biol. *14*, 5165–5174.

Debuchy, R., Purton, S., and Rochaix, J.D. (1989). The argininosuccinate lyase gene of *Chlamydomonas reinhardtii*: an important tool for nuclear transformation and for correlating the genetic and molecular maps of the *ARG7* locus. EMBO J. *10*, 2803–2809.

Dutcher, S.K. (1995). Flagellar assembly in two hundred and fifty easy-to-follow steps. Trends Genet. *11*, 398–404.

Ebersold, W.T. (1967). *Chlamydomonas reinhardtii*: heterozygous diploid strains. Science *157*, 446–449.

Gardner, L.C., O'Toole, E., Perrone, C.A., Giddings, T., and Porter, M.E. (1994). Components of a "dynein regulatory complex" are located at the junction between the radial spokes and the dynein arms in *Chlamydomonas* flagella. J. Cell Biol. *127*, 1311–1325.

Gee, M.A., Heuser, J.E., and Vallee, R.B. (1997). An extended microtubule-binding structure within the dynein motor domain. Nature *390*, 636–639.

Gibbons, B.H., Asai, D.J., Tang, W.J., Hays, T.S., and Gibbons, I.R. (1994). Phylogeny and expression of axonemal and cytoplasmic dynein genes in sea urchins. Mol. Biol. Cell *5*, 57–70.

Gibbons, I.R. (1995). Dynein family of motor proteins: present status and future questions. Cell Motil. Cytoskeleton *32*, 136–144.

Goodenough, U.W. (1992). Green yeast. Cell *70*, 533–538.

Goodenough, U.W., Gebhart, B., Mermall, V., Mitchell, D.R., and Heuser, J.E. (1987). High pressure liquid chromatography fractionation of *Chlamydomonas* dynein extracts and characterization of inner arm dynein subunits. J. Mol. Biol. *194*, 481–494.

Habermacher, G., and Sale, W.S. (1996). Regulation of a flagellar dynein by axonemal type-1 phosphatase in *Chlamydomonas*. J. Cell Sci. *109*, 1899–1907.

Habermacher, G., and Sale, W.S. (1997). Regulation of flagellar dynein by phosphorylation of a 138-kD inner arm dynein intermediate chain. J. Cell Biol. *136*, 167–176.

Habura, A., Tikhonenko, I., Chisholm, R.L., and Koonce, M.P. (1999). Interaction mapping of a dynein heavy chain: identification of dimerization and intermediate-chain binding domains. J. Biol. Chem. *274*, 15447–15453.

Harris, E. (1989). The *Chlamydomonas* Sourcebook, San Diego, CA: Academic Press.

Harrison, A., Olds-Clarke, P., and King, S.M. (1998). Identification of the *t* complex-encoded cytoplasmic dynein light chain Tctex1 in inner arm I1 supports the involvement of flagellar dyneins in meiotic drive. J. Cell Biol. *140*, 1137–1147.

Herrmann, B.G., Koschorz, B., Wertz, K., McLaughlin, K.J., and Kispert, A. (1999). A protein kinase encoded by the *t complex responder* gene cause non-mendelian inheritance. Nature *402*, 141–146.

Hirokawa, N., Noda, Y., and Okada, Y. (1998). Kinesin and dynein superfamily proteins in organelle transport and cell division. Curr. Opin. Cell Biol. *10*, 60–73.

Inaba, K., Kagami, O., and Ogawa, K. (1999). Tctex2-related outer arm dynein light chain is phosphorylated at activation of sperm motility. Biochem. Biophys. Res. Commun. *256*, 177–183.

Iyadurai, S.J., Li, M.G., Gilbert, S.P., and Hays, T.S. (1999). Evidence for cooperative interactions between the two motor domains of cytoplasmic dynein. Curr. Biol. *9*, 771–774.

Kagami, O., and Kamiya, R. (1992). Translocation and rotation of microtubules caused by multiple species of *Chlamydomonas* inner-arm dynein. J. Cell Sci. *103*, 653–664.

Kamiya, R., Kurimoto, E., and Muto, E. (1991). Two types of *Chlamydomonas* flagellar mutants missing different components of inner-arm dynein. J. Cell Biol. *112*, 441–447.

Kindle, K.L. (1990). High-frequency nuclear transformation of *Chlamydomonas reinhardtii*. Proc. Natl. Acad. Sci. USA *87*, 1228–1232.

King, S.J., and Dutcher, S.K. (1997). Phosphoregulation of an inner dynein arm complex in *Chlamydomonas reinhardtii* is altered in phototactic mutant strains. J. Cell Biol. *136*, 177–191.

King, S.M., Babarese, E., Dillman, J.F., III, Benashski, S.E., Do, K.T., Patel-King, R., and Pfister, K.K. (1998). Cytoplasmic dynein contains a family of differentially expressed light chains. Biochemistry *37*, 15033–15041.

King, S.M., Dillman, J.F., III, Benashski, S.E., Lye, R.J., Patel-King, R.S., and Pfister, K.K. (1996). The mouse *t* complex-encoded protein Tctex1 is a light chain of brain cytoplasmic dynein. J. Biol. Chem. *271*, 32281–32287.

King, S.M., and Patel-King, R.S. (1995). The M(r) = 8,000 and 11,000 outer arm dynein light chains from *Chlamydomonas* flagella have cytoplasmic homologues. J. Biol. Chem. *270*, 11445–11452.

Koonce, M.P. (1997). Identification of a microtubule-binding domain in a cytoplasmic dynein heavy chain. J. Biol. Chem. *272*, 19714–19718.

Koonce, M.P., Grissom, P.M., and McIntosh, J.R. (1992). Dynein from *Dictyostelium*: primary structure comparisons between a cytoplasmic motor enzyme and flagellar dynein. J. Cell Biol. *119*, 1597–1604.

Koonce, M.P., and Knecht, D.A. (1998). Cytoplasmic dynein heavy chain is an essential gene product in *Dictyostelium*. Cell Motil. Cytoskeleton *39*, 63–72.

Lader, E., Ha, H.-S., O'Neill, M., Artzt, K., and Bennett, D. (1989). *tctex*-1: a candidate gene family for a mouse *t* complex sterility locus. Cell *58*, 969–979.

LeDizet, M., and Piperno, G. (1995). *ida4-1*, *ida4-2*, and *ida4-3* are intron splicing mutations affecting the locus encoding p28, a light chain of *Chlamydomonas* axonemal inner dynein arms. Mol. Biol. Cell *6*, 713–723.

Lupus, A. (1996). Prediction and analysis of coiled-coil structures. Methods Enzymol. *266*, 513–525.

Lupus, A., Van Dyke, M., and Stock, J. (1991). Predicting coiled coils from protein sequences. Science *252*, 1162–1164.

Lyon, M.F. (1984). Transmission ratio distortion in mouse *t*-haplotypes is due to multiple distorter genes acting on a responder locus. Cell *37*, 621–628.

Lyon, M.F. (1986). Male sterility of the mouse *t*-complex is due to homozygosity of the distorter genes. Cell *44*, 357–363.

Mastronarde, D.N., O'Toole, E.T., McDonald, K.L., McIntosh, J.R., and Porter, M.E. (1992). Arrangement of inner dynein arms in wild-type and mutant flagella of. *Chlamydomonas*. J. Cell Biol. *118*, 1145–1162.

Mitchell, D.R. (1994). Cell and molecular biology of flagellar dyneins. Int. Rev. Cytol. *155*, 141–175.

Mitchell, D.R., and Brown, K.S. (1994). Sequence analysis of the *Chlamydomonas* α and β dynein heavy chain genes. J. Cell Sci. *107*, 635–644.

Mitchell, D.R., and Brown, K.S. (1997). Sequence analysis of the *Chlamydomonas reinhardtii* flagellar α dynein gene. Cell Motil. Cytoskeleton *37*, 120–126.

Mitchell, D.R., and Rosenbaum, J.L. (1985). A motile *Chlamydomonas* flagellar mutant that lacks the outer dynein arms. J. Cell. Biol. *100*, 1228–1234.

Myster, S.H., Knott, J.A., O'Toole, E., and Porter, M.E. (1997). The *Chlamydomonas Dhc1* gene encodes a dynein heavy chain subunit required for assembly of the I1 inner arm complex. Mol. Biol. Cell *8*, 607–620.

Myster, S.H., Knott, J.A., Wysocki, K.M., O'Toole, E., and Porter, M.E. (1999). Domains in the 1-alpha dynein heavy chain required for inner arm assembly and flagellar motility in *Chlamydomonas*. J. Cell Biol. *146*, 801–818.

Nagano, F., Orita, S., Sasaki, T., Naito, A., Sakaguchi, G., Maeda, M., Watanabe, T., Kominami, E., Uchiyama, Y., and Takai, Y. (1998). Interaction of Doc2 with Tctex1, a light chain of cytoplasmic dynein. J. Biol. Chem. *273*, 30065–30068.

Nakamura, Y., Gojobori, T., and Ikemura, T. (1997). Codon usage tabulated from the international DNA sequence databases. Nucleic Acids Res. *25*, 244–245.

Nelson, J.A., and Lefebvre, P.A. (1995). Transformation of *Chlamydomonas reinhardtii*. Methods Cell Biol.*47*, 513–517.

Neuwald, A.F., Aravind, L., Spouge, J.L., and Koonin, E.V. (1999). AAA+: a class of chaperone-like ATPases associated with the assembly, operation, and disassembly of protein complexes. Genome Res. *9*, 27–43.

Olds-Clarke, P. (1997). Models for male infertility: the *t* haplotypes. Rev. Reprod. *2*, 157–164.

O'Toole, E., Mastronarde, D., McIntosh, J.R., and Porter, M.E. (1995). Computer-assisted image analysis of flagellar mutants. Methods Cell Biol. *47*, 183–191.

Patel-King, R.S., Benashski, S.E., Harrison, A., and King, S.M. (1997). A *Chlamydomonas* homologue of the putative murine *t* complex distorter Tctex-2 is an outer arm dynein light chain. J. Cell Biol. *137*, 1081–1090.

Pazour, G.J., Wilkerson, C.G., and Witman, G.B. (1998). A dynein light chain is essential for the retrograde particle movement of intraflagellar transport (IFT). J. Cell Biol. *141*, 979–992.

Perrone C.A., Yang, P., O'Toole, E., Sale, W.S., and Porter, M.E. (1998). The *Chlamydomonas IDA7* locus encodes a 140-kDa dynein intermediate chain required to assemble the I1 inner arm complex. Mol. Biol. Cell *9*, 3351–3365.

Piperno, G., Ramanis, Z., Smith, E.F., and Sale, W.S. (1990). Three distinct inner dynein arms in *Chlamydomonas* flagella: molecular composition and location in the axoneme. J. Cell Biol. *110*, 379–389.

Porter, M.E. (1996). Axonemal dyneins: assembly, organization, and regulation. Curr. Opin. Cell Biol. *8*, 10–17.

Porter, M.E., Bower, R., Knott, J.A., Byrd, P., and Dentler, W. (1999). Cytoplasmic dynein heavy chain 1b is required for flagellar assembly in *Chlamydomonas*. Mol. Biol. Cell *10*, 693–712.

Porter, M.E., Knott, J.A., Myster, S.H., and Farlow, S.J. (1996). The dynein gene family in *Chlamydomonas reinhardtii*. Genetics *144*, 569–585.

Porter, M.E., Power, J., and Dutcher, S.K. (1992). Extragenic suppressors of paralyzed flagellar mutations in *Chlamydomonas reinhardtii* identify loci that alter the inner dynein arms. J. Cell Biol. *118*, 1163–1176.

Sakakibara, H., Takada, S., King, S.M., Witman, G.B., and Kamiya, R. (1993). A *Chlamydomonas* outer arm dynein mutant with a truncated beta heavy chain. J. Cell. Biol. *122*, 653–661.

Schnell, R.A., and Lefebvre, P.A. (1993). Isolation of the *Chlamydomonas* regulatory gene *NIT2* by transposon tagging. Genetics *134*, 737–747.

Silflow, C.D. (1998). Organization of the nuclear genome. *In* The Molecular Biology of Chloroplasts and Mitochondria in *Chlamydomonas*, ed. J.-D. Rochaix, M. Goldschmidt-Clermont, and S. Merchant, Dordrecht, The Netherlands: Kluwer Academic Publishers, 25–40.

Silver, L.M. (1993). The peculiar journey of a selfish chromosome: mouse *t* haplotypes and meiotic drive. Trends Genet. *9*, 250–254.

Smith, E.F., and Sale, W.S. (1992). Structural and functional reconstitution of inner dynein arms in *Chlamydomonas* flagellar axonemes. J. Cell Biol. *117*, 573–581.

Tai, A.W., Chuang, J.Z., Bode, C., Wolfrum, U., and Sung, C.H. (1999). Rhodopsin's carboxy-terminal cytoplasmic tail acts as a membrane receptor for cytoplasmic dynein by binding to the dynein light chain Tctex1. Cell *97*, 877–887.

Tai, A.W., Chuang, J.Z., and Sung, C.H. (1998). Localization of Tctex1, a cytoplasmic dynein light chain, to the Golgi apparatus and evidence for dynein complex heterogeneity. J. Biol. Chem. *31*, 19639–19649.

Takada, S., and Kamiya, R. (1994). Functional reconstitution of the inner dynein arms in *Chlamydomonas* flagellar axonemes. J. Cell Biol. *131*, 399–409.

Tam, L.W., and Lefebvre, P.A. (1993). Cloning of flagellar genes in *Chlamydomonas reinhardtii* by DNA insertional mutagenesis. Genetics *135*, 375–384.

Tanaka, Y., Zhang, Z., and Hirokawa, N. (1995). Identification and molecular evolution of new dynein-like protein sequences in rat brain. J. Cell Sci. *108*, 1883–1893.

Walker, J.E., Saraste, M., Runswick, M.J., and Gay, N.J. (1982). Distantly related sequences in the alpha- and beta-subunits of ATP synthase, myosin, kinases and other ATP-requiring enzymes and a common nucleotide binding fold. EMBO J. *1*, 945–951.

Wilkerson, C.G., King, S.M., Koutoulis, A., Pazour, G.J., and Witman, G.B. (1995). The 78,000 M(r) intermediate chain of *Chlamydomonas* outer arm dynein is a WD-repeat protein required for arm assembly. J. Cell Biol. *129*, 169–178.

Wilkerson, C.G., King, S.M., and Witman, G.B. (1994). Molecular analysis of the γ heavy chain of *Chlamydomonas* flagellar outer arm dynein. J. Cell Sci. *107*, 497–506.

Wray, W., Boulikas, T., Wray, V.P., and Hancock, R. (1981). Silver staining of proteins in polyacrylamide gels. Anal. Biochem. *118*, 197–203.

Yang, P., Fox, L., Colbran, R.J., and Sale, W.S. (2000). Protein phosphatases PP1 and PP2A are located in distinct positions in the *Chlamydomonas* flagellar axoneme. J. Cell Sci. *113*, 91–102.

Yang, P., and Sale, W.S. (1998). The Mr 140,000 intermediate chain of *Chlamydomonas* flagellar inner arm dynein is a WD-repeat protein implicated in dynein arm anchoring. Mol. Biol. Cell *9*, 3335–3349.

Yang, P., and Sale, W.S. (1999). An axonemal CKI (casein kinase I) regulates flagellar dynein. Mol. Biol. Cell *10*, S389a.

Zhang, D. (1996). Regulation of Nitrate Assimilation in *Chlamydomonas reinhardtii*. Ph.D. Thesis. Minneapolis, MN: University of Minnesota.